CHAPTER 4

Forced fusion of human ventricular scar cells with cardiomyocytes suppresses arrhythmogenicity in a co-culture model

Marc C. Engels[1,†], Saïd F.A. Askar[1,†], Wanchana Jangsangthong[1]; Brian O. Bingen[1], Iolanda Feola[1], Jia Liu[1], Rupamanjari Majumder[1], Michel I.M. Versteegh[2], Jerry Braun[2], Robert J.M. Klautz[2], Dirk L. Ypey[1], Antoine A.F. de Vries[1,†], Daniël A. Pijnappels[1,†]

[†]These authors contributed equally to this work.

Laboratory of Experimental Cardiology[1], Department of Cardiology, and Department of Cardiothoracic Surgery[2], Heart Lung Center Leiden, Leiden University Medical Center, Leiden, the Netherlands.

Adapted from: Cardiovascular Research. 2015;107:601-612.

Abstract

Aims: Fibrosis increases arrhythmogenicity in myocardial tissue by causing structural and functional disruptions in the cardiac syncytium. Forced fusion of fibroblastic cells with adjacent cardiomyocytes may theoretically resolve these disruptions. Therefore, the electrophysiological effects of such electrical and structural integration of fibroblastic cells into a cardiac syncytium were studied.

Methods and results: Human ventricular scar cells (hVSCs) were transduced with lentiviral vectors encoding enhanced green fluorescent protein alone (eGFP↑-hVSCs) or together with the fusogenic vesicular stomatitis virus-G protein (VSV-G/eGFP↑-hVSCs) and subsequently co-cultured (1:4 ratio) with neonatal rat ventricular cardiomyocytes (NRVMs) in confluent monolayers yielding eGFP↑- and VSV-G/eGFP↑-co-cultures, respectively. Cellular fusion was induced by brief exposure to pH = 6.0 medium. Optical mapping experiments showed eGFP↑-co-cultures to be highly arrhythmogenic (43.3% early afterdepolarization [EAD] incidence vs. 7.7% in control NRVM cultures, $P < 0.0001$), with heterogeneous prolongation of action potential (AP) duration (APD). Fused VSV-G/eGFP↑-co-cultures displayed markedly lower EAD incidence (4.6%, $P < 0.001$) than unfused co-cultures, associated with decreases in APD, APD dispersion, and decay time of cytosolic Ca^{2+} waves. Heterokaryons strongly expressed connexin43 (Cx43). Also, maximum diastolic potential in co-cultures was more negative after fusion, while heterokaryons exhibited diverse mixed NRVM/hVSC whole-cell current profiles, but consistently showed increased outward K_v currents compared with NRVMs or hVSCs. Inhibition of K_v channels by tetraethylammonium chloride abrogated the anti-arrhythmic effects of fusion in VSV-G/eGFP↑-co-cultures raising EAD incidence from 7.9% to 34.2% ($P < 0.001$).

Conclusion: Forced fusion of cultured hVSCs with NRVMs yields electrically functional heterokaryons and reduces arrhythmogenicity by preventing EADs, which is, at least partly, attributable to increased repolarization force.

Introduction

While cardiomyocytes (CMCs) are responsible for the coordinated contraction of the heart by forming a functional syncytium of contractile cells via an extensive network of gap and adherent junctions, cardiac fibroblasts (CFBs) play a crucial supportive role.[1] Interactions between CMCs and CFBs are not only important for the optimal functioning of the healthy heart, but also play a major role in the adaptation to pathological conditions.[2,3] For example, after myocardial infarction, the number of fibroblastic cells at the site of injury increases significantly, resulting in scar formation. While scar formation ensures cardiac integrity after damage, in the long run cardiac fibrosis negatively affects both the electrical and mechanical performance of the heart.[4]

Cardiac fibrosis is a process of adaptation and repair involving replacement of damaged CMCs by fibrous tissue in response to injury (e.g. myocardial infarction), disease, and aging, which creates an imbalance between parenchymal and interstitial cells. Moreover, cardiac fibrosis increases tissue heterogeneity as it causes local accumulation of fibroblastic cells (particularly myofibroblasts) and excessive deposition of extracellular matrix, potentially disrupting normal conduction pathways. Cardiac fibrosis may also affect cardiac ion transporters and Ca^{2+}-handling proteins through crosstalk between CMCs and cardiac (myo)fibroblasts.[5] As a result of the disruptive effects of scar fibroblasts on the cardiac syncytium, electrical impulse generation and propagation could become disturbed, leading to an increased pro-arrhythmic risk in fibrotic myocardium.[6]

Although several studies have focused on the mechanisms underlying arrhythmia initiation and dynamics in fibrotic substrates[7-9], relatively few studies have been undertaken to restore the interrupted electrical syncytium.[10] An obvious strategy to reduce the arrhythmogenicity associated with cardiac fibrosis, is to normalize as much as possible tissue composition, structure, and function and thereby reduce electrical heterogeneity. This goal may be achieved by increasing the number of excitable and/or well-coupled cells or by improving the electrophysiological properties of resident, non-excitable, poorly coupled fibroblastic cells. Both cell and gene therapy have been employed to reduce electrical heterogeneity at sites of cardiac injury.[11] Impaired electrical impulse generation and propagation in fibrotic myocardium can indeed be improved by transplantation of stem cell-derived CMCs, thereby lowering pro-arrhythmic risk,[12] although opposite findings have also been reported.[13] More direct approaches to improve electrophysiological function of fibrotic myocardium through genetic modification of cardiac (myo)fibroblasts have also been pursued, such as manipulation of their ion channel and/or gap junction protein expression levels.[10,14] Also, direct

cardiomyogenic transdifferentiation of (myo)fibroblasts via transcription factor- or microRNA-based reprogramming has been explored as a strategy to convert fibroblasts into CMCs.[15] Although theoretically this approach may succeed in restoring the electrophysiological balance in fibrotic hearts, cardiomyogenic reprogramming of cardiac (myo)fibroblasts is still inefficient and incomplete.[16]

From a conceptual point of view, merging of myocardial scar cells into the cardiac syncytium may represent a mechanistically new approach to reduce fibrosis-related arrhythmogenicity. Therefore, in this study, the electrophysiological effects of integrating fibroblastic cells into the cardiac syncytium by forced heterocellular fusion were investigated. To this purpose, human ventricular scar cells (hVSCs) were endowed with controllable membrane fusion capacity by transduction with a lentivirus vector (LV) encoding the vesicular stomatitis virus G protein (VSV-G).[17]

Methods

Expanded methods descriptions are available in the Supplementary material online.
Human tissue was collected in accordance with guidelines posed by the Medical Ethics Committee of Leiden University Medical Center (LUMC), which follow the principles described in the Declaration of Helsinki. All animal experiments were approved by LUMC's Animal Experiments Committee and conformed to the Guide for the Care and Use of Laboratory Animals as stated by the US National Institutes of Health.

Isolation, culture, and transduction of hVSCs

hVSCs were isolated from surgical waste material consisting of myocardial scar tissue of patients undergoing left ventricular reconstructive surgery (n = 10) and cultured as described previously.[10,18] Cells from all 10 patients were pooled and used at passage number 2-4 for further experiments. hVSCs were transduced with LVs encoding enhanced green fluorescent protein (eGFP) and the fusogenic VSV-G (LV.VSV-G/eGFP↑) or eGFP alone (LV.eGFP↑) to generate VSV-G/eGFP↑-hVSCs and eGFP↑-hVSCs, respectively.

Neonatal rat ventricular myocyte isolation and co-culture

Neonatal rat ventricular myocytes (NRVMs) were isolated as described previously.[19] Briefly, neonatal Wistar rats (2 days *post-partum*) were anaesthetized by 5% isoflurane inhalation, and adequate anaesthesia was confirmed by the absence of reflexes. Next, hearts were rapidly excised, and ventricles were finely minced and dissociated with collagenase type 1 (450 U/

mL; Worthington, Lakewood, NJ, USA) and DNase I (18.75 Kunitz/mL; Sigma-Aldrich, St. Louis, MO, USA). After selective depletion of most fibroblastic cells by pre-plating, the remaining cells (mainly CMCs) were mixed with hVSCs in a ratio of 4:1 for all co-culture groups and seeded on fibronectin-coated (Sigma-Aldrich) coverslips in 24-well plates (Corning Life Sciences, Corning, NY, USA). Co-cultures were established with untransduced hVSCs (UT-co-cultures), VSV-G/eGFP↑-hVSCs (VSV-G/eGFP↑-co-cultures) or eGFP↑-hVSCs (eGFP↑-co-cultures). NRVM cultures without hVSCs (hereinafter referred to as NRVM cultures) were taken along as control whenever indicated. Cells were plated at a total density of 0.5-6 $\times$ 10^5 cells/well, depending on the assay. Twelve to 16 hours after plating, cultures were treated for 2 h with mitomycin-C (10 µg/mL; Sigma-Aldrich) to prevent proliferation of non-CMCs.[19]

Induction and assessment of cell-to-cell fusion

To induce intercellular fusion, cells were incubated with sodium 2-(4-morpholino-) ethanesulfonate-buffered (Sigma-Aldrich) NRVM culture medium of pH 6.0 for 3.5 min at 37°C in water vapour-saturated 95% air/5% CO_2 on Day 3 of co-culture. All co-cultures, including those containing untransduced hVSCs and eGFP↑-hVSCs and NRVM cultures underwent the same treatment unless indicated otherwise. Fusion efficiency was assessed by immunocytological assay and by phase contrast microscopy. Phase contrast analysis was done on Day 4 of co-culture (*i.e.* 24 h after induction of intercellular fusion) using a Carl Zeiss Axiovert 40C microscope. For each culture, 10 random fields of view were analysed. The total number of nuclei in each field of view was counted, as well as the total number of nuclei in heterokaryons (*i.e.* cells containing > 2 nuclei). The percentage of heterokaryonic nuclei per field of view was calculated and averaged for the 10 fields of view inspected per experimental group. VSV-G/eGFP↑-co-cultures were included for further assay when 40-60% of the nuclei were in heterokaryons.

Optical voltage mapping

Assessment of the electrophysiological effects of heterocellular fusion was performed by optical voltage mapping as described previously.[20] On Day 5 of co-culture, cells were loaded with potentiometric dye by incubation for 15 min at 37°C with colourless HEPES-buffered DMEM/F12 containing 8 µM di-4-ANEPPS (both from Life Technologies, Carlsbad, CA, USA), and optically mapped using a MiCAM ULTIMA-L imaging system (SciMedia USA, Costa Mesa, CA, USA). To study the effect of K_v current inhibition, cultures were optically mapped after a 10-min incubation with 40 mM tetraethylammonium chloride (TEA; Sigma-Aldrich) or 1 mM 4-aminopyridine (4-AP; Sigma-Aldrich) at 37°C.

Optical mapping of Ca^{2+} dynamics

Intracellular Ca^{2+} dynamics were assessed by optical mapping with the Ca^{2+}-sensitive dye Rhod-2-AM (Life Technologies). Cells were labelled by incubation with 2.5 μM Rhod-2-AM in DMEM/F12 at 37°C for 30 min. Next, cells were incubated in fresh, unsupplemented DMEM/F12 for another 30 min in the incubator for de-esterification of internalized Rhod-2-AM. Optical signals were captured using the MiCAM ULTIMA-L imaging system. Cells were stimulated electrically at a frequency of 1-Hz. As a quantitative measure of Ca^{2+} dynamics, the time for the signal to decrease to 63% of the peak value was determined using BrainVision Analyzer 1101 software (Brainvision, Tokyo, Japan).

Transwell assays

The effects of paracrine signaling of hVSCs on the electrophysiological properties of NRVMs was assessed by transwell assays. NRVMs were cultured as described previously, plated at a density of 6×10^5 cells/well on fibronectin-coated, 15-mm diameter, round glass coverslips and placed at the bottom of 24-well transwell plates (Corning Life Sciences). The transwell inserts (0.4 μm pore size) were seeded with hVSCs (1.5×10^5 cells/insert) or were left unseeded to provide negative controls. Cells were cultured in NRVM culture medium, which was refreshed every 48 h to allow ample exposure to paracrine factors. At Day 5 of culture, optical mapping experiments were performed as described above. To investigate the possibility of acute paracrine effects during optical mapping experiments, hVSC-seeded or empty inserts were cultured in DMEM/F12 for 48 h, after which the culture medium was collected. This conditioned medium (CM) was subsequently used for potentiometric dye loading and during optical mapping.

Patch-clamp recordings

Patch-clamp measurements were conducted on Day 5 of (co-)culture with a conventional system consisting of a MultiClamp 700B amplifier and a Digidata 1440A A/D converter, controlled by Clampex 10 software (Axon CNS, Molecular Devices, Sunnyvale, CA, USA), as previously described.[21] Current- and voltage-clamp recordings were performed on single NRVMs, single hVSCs, and solitary heterokaryons. In addition, perforated patch-clamp recordings on NRVMs in confluent NRVM cultures, NRVMs adjacent to eGFP↑-hVSCs in confluent eGFP↑-co-cultures and heterokaryons in confluent VSV-G/eGFP↑-co-cultures were also performed to examine the AP characteristics in these cultures. Data sets were derived from ≥3 independent experiments.

Statistical analysis

Statistical analyses were performed using GraphPad Prism software version 6 (Graphpad Software, La Jolla, CA, USA). Unpaired Student's *t*-test, Fisher's exact test and one-way analysis of variance (ANOVA) with Bonferroni's multiple comparison test were used for comparisons

between experimental groups. Data were expressed as mean ± standard error of mean (SEM) for a specified number (*n*) of observations with each observation representing an independent culture or cell. Results were considered statistically significant at *P*-values < 0.05. Statistical significance was expressed as follows: *$P < 0.05$, **$P < 0.001$, NS: not significant.

Results

Co-culture of NRVMs with hVSCs is pro-arrhythmic

Immunocytological staining showed that all hVSCs were positive for collagen type 1 (COL1), but negative for smooth muscle myosin heavy chain (sm-MHC), sarcomeric alpha-actinin (ACTN), and platelet endothelial cell adhesion molecule (PECAM-1). Of the $COL1^+$ cells, roughly 40% were alpha smooth muscle actin (α-SMA)-positive (see Supplementary material online, *Figure S1*). Phase contrast microscopy showed that NRVM cultures, as well as UT-co-cultures, formed confluent monolayers. Immunocytogical analyses confirmed a 4:1 ratio of NRVMs ($ACTN^+$ cells) and hVSCs (human lamin A/C [$hLMNA^+$] cells) in UT-co-cultures (*Figure 1A*). Optical voltage mapping of 1-Hz electrically stimulated cultures indicated a significantly lower conduction velocity (CV) in UT-co-cultures than in NRVM cultures (*Figure 1B*). Both NRVM and UT-co-cultures typically displayed 1:1 uniform convex propagation originating from the bipolar pacing electrode (*Figure 1C*). UT-co-cultures typically featured increases in action potential (AP) duration (APD; *Figure 1D* and *E*) and APD_{80} dispersion (*Figure 1F*). This was associated with a much higher early afterdepolarization (EAD) incidence upon 1-Hz stimulation in UT-co-cultures compared with NRVM cultures (*Figure 1G* and *H*). These data indicate that addition of hVSCs to NRVM cultures greatly increases their arrhythmogenicity.

To investigate whether paracrine signaling of hVSCs could render NRVM cultures pro-arrhythmic, hVSCs were cultured on a cell-impermeable membrane above NRVMs using transwell culture plates. These studies showed no significant difference in CV, APD_{80}, APD_{80} dispersion, and EAD incidence between NRVM cultures that had, and NRVM cultures that had not been exposed to paracrine factors released by hVSCs (Supplementary material online, *Figure S2*). Paracrine signalling by hVSCs thus seems not to be a major contributor to the high arrhythmogenicity of NRVM-hVSC co-cultures.

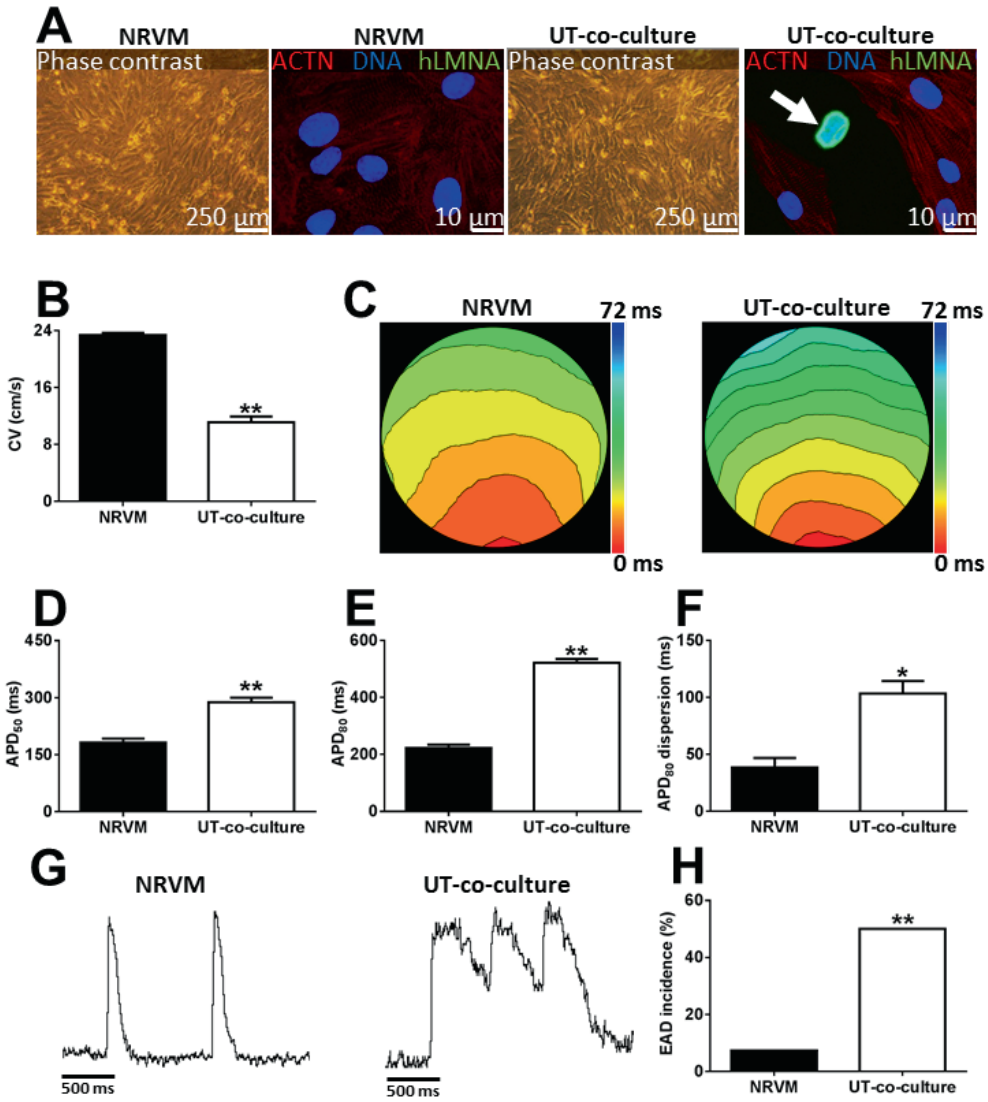

Figure 1. NRVM-hVSC-co-cultures display a pro-arrhythmic phenotype. (*A*) Typical examples of phase-contrast microscopic images and immunocytological stainings of NRVM cultures (**left panels**) and UT-co-cultures, which contained NRVMs and untransduced hVSCs (**right panels**) in a 4:1 ratio. Cells were stained for sarcomeric α-actinin (ACTN, red, NRVMs), human lamin A/C (hLMNA, green, hVSCs) and with Hoechst 33342 (DNA, blue, nuclei). The white arrow indicates an $hLMNA^+$ hVSC nucleus. (*B*) Assessment of CV by optical mapping. (*C*) Representative activation maps (6-ms isochrone spacing) of NRVM culture **(left)** and UT-co-culture **(right)** paced at 1 Hz. Quantification of (*D*) APD_{50}, (*E*) APD_{80} and (*F*) APD_{80} dispersion. (*G*) Typical optical signal trace during 1-Hz electrical stimulation of an NRVM culture **(left)** and an EAD-displaying UT-co-culture **(right)**. (*H*) Quantification of EAD incidence. Quantitative data were based on 41 NRVM cultures and 46 UT-co-cultures.

Characterization of heterokaryonic fusion products

hVSCs were transduced with LV.eGFP↑ (*Figure 2A*; control vector) to generate hVSCs that were only eGFP$^+$ (eGFP↑-hVSCs; Supplementary material, *Figure S3A*), or with LV.VSV-G/eGFP↑ (*Figure 2B*) to generate hVSCs expressing both VSV-G and eGFP (VSV-G/eGFP↑-hVSCs; Supplementary material, *Figure S3B*). The transduced cells were then co-cultured with NRVMs. Brief exposure of these co-cultures to pH= 6.0 medium caused the VSV-G/eGFP↑-hVSCs, but not the eGFP↑-hVSCs, to fuse with surrounding NRVMs (*Figure 2C* and *D*). Immunostaining of eGFP↑-co-cultures showed the presence of ACTN$^+$/hLMNA$^-$ cells (NRVMs) and of cells that were positive for COL1 and hLMNA (hVSCs; *Figure 2C*). However, after induction of fusion in VSV-G/eGFP↑-co-cultures, large multinucleated cells were observed, which were positive for COL1 as well as for ACTN, confirming fusion of hVSCs with NRVMs into heterokaryons (*Figure 2D*). These cells contained on average 11.0±0.8 nuclei, of which 22.5±1.3% were positive for hLMNA (*Figure 2E*). The VSV-G/eGFP↑-co-cultures did not show signs of apoptosis at 2, 4 or 6 after fusion induction, as assessed by annexin V live cell staining (Supplementary material, *Figure S4*).

To further study the electrophysiological characteristics of heterokaryons at a functional level, patch-clamp experiments were performed on single NRVMs, single hVSCs and isolated heterokaryons. As expected, short depolarizing current-clamp stimulations (5 ms, 100-300 pA) were sufficient to evoke APs in NRVMs (*Figure 3A)*, but failed to initiate APs in hVSCs. The spiky response of hVSCs to the current stimulus reflects their inexcitability, as the response curve follows the discharge characteristics of a passive resistance-capacitance circuit *(Figure 3B*). Under our experimental conditions, 1 out 2 heterokaryons (hereinafter referred to as responsive heterokaryons) readily elicited an AP upon stimulation (*Figure 3C*). Maximal upstroke velocity was 38.0±5.9 mV/ms for responsive heterokaryons, compared to 88.0±13.2 mV/ms for NRVMs (*Figure 3D*). AP amplitude did not significantly differ between these heterokaryons and NRVMs (*Figure 3E*), while the average APD_{80} of responsive heterokaryons was considerably longer than that of NRVMs (480.6±90.2 ms vs. 110.9±8.0 ms, $P<0.0022$, N=10 and 8, respectively). Furthermore, responsive heterokaryons had a resting membrane potential in between that of unfused hVSCs and NRVMs (*Figure 3F*). Being derived from multiple cells, heterokaryons possessed a larger cell membrane capacitance (C_m) than individual NRVMs or hVSCs (*Figure 3G*). These data indicate that forced heterocellular fusion yields electrically functional heterokaryons.

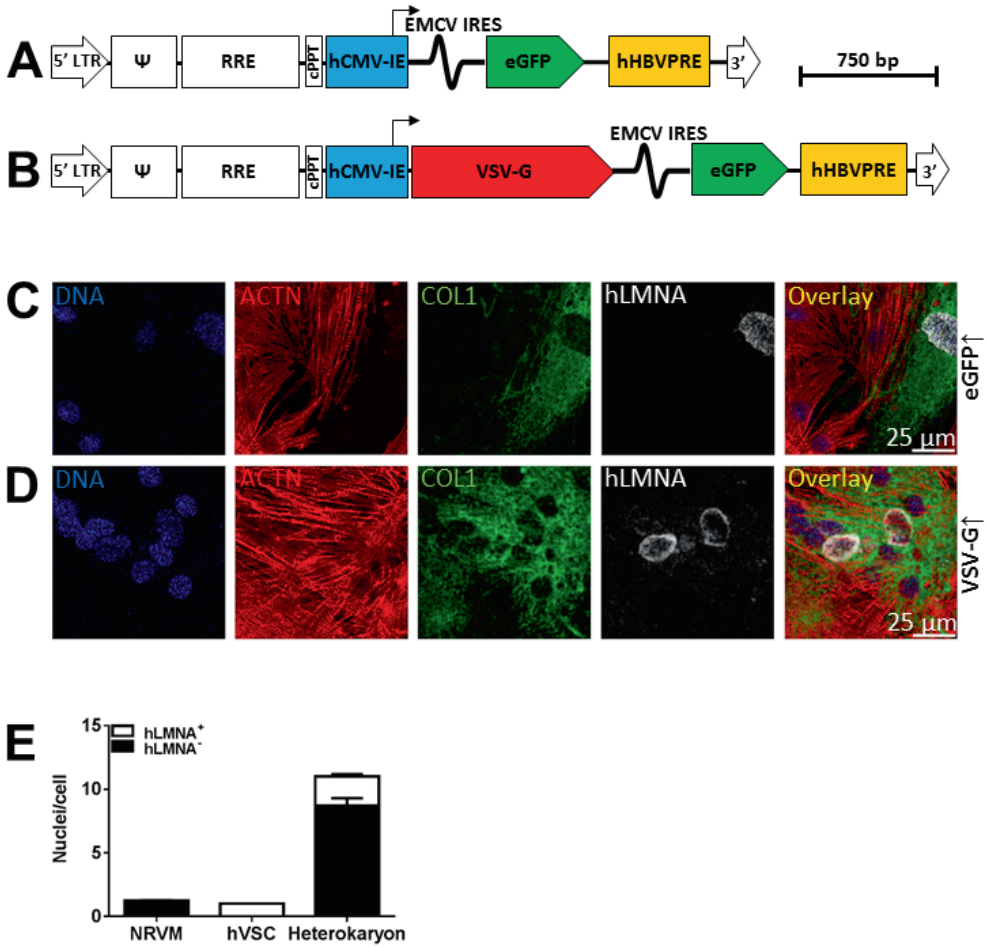

Figure 2. VSV-G-mediated heterocellular fusion of hVSCs with NRVMs. Proviral DNA structure of (*A*) LV.eGFP↑ and (*B*) LV.VSV-G/eGFP↑. The different abbreviations are explained in the chapter designated "Construction of self-inactivating lentiviral vector (SIN-LV) shuttle plasmids" of the Supplementary material. Co-culture containing hVSCs transduced with either (*C*) LV.eGFP↑ (eGFP↑-co-culture; eGFP↑) or (*D*) LV.VSV-G/eGFP↑ (VSV-G/eGFP-↑-co-culture; VSV-G↑) upon brief exposure to pH 6. Cells were stained for sarcomeric α-actinin (ACTN, red, NRVMs), collagen type I (COL1, green, hVSCs), human lamin A/C (hLMNA, white, hVSCs) and Hoechst 33342 (DNA, blue, nuclei). (*E*) Quantification of total number of nuclei and their origin per cell for NRVMs (N=31), hVSCs (N=28) and heterokaryons (N=53), as assessed by immunocytological staining. Human nuclei were distinguished from rat nuclei by their positive staining for hLMNA. Scale bar=25 µm.

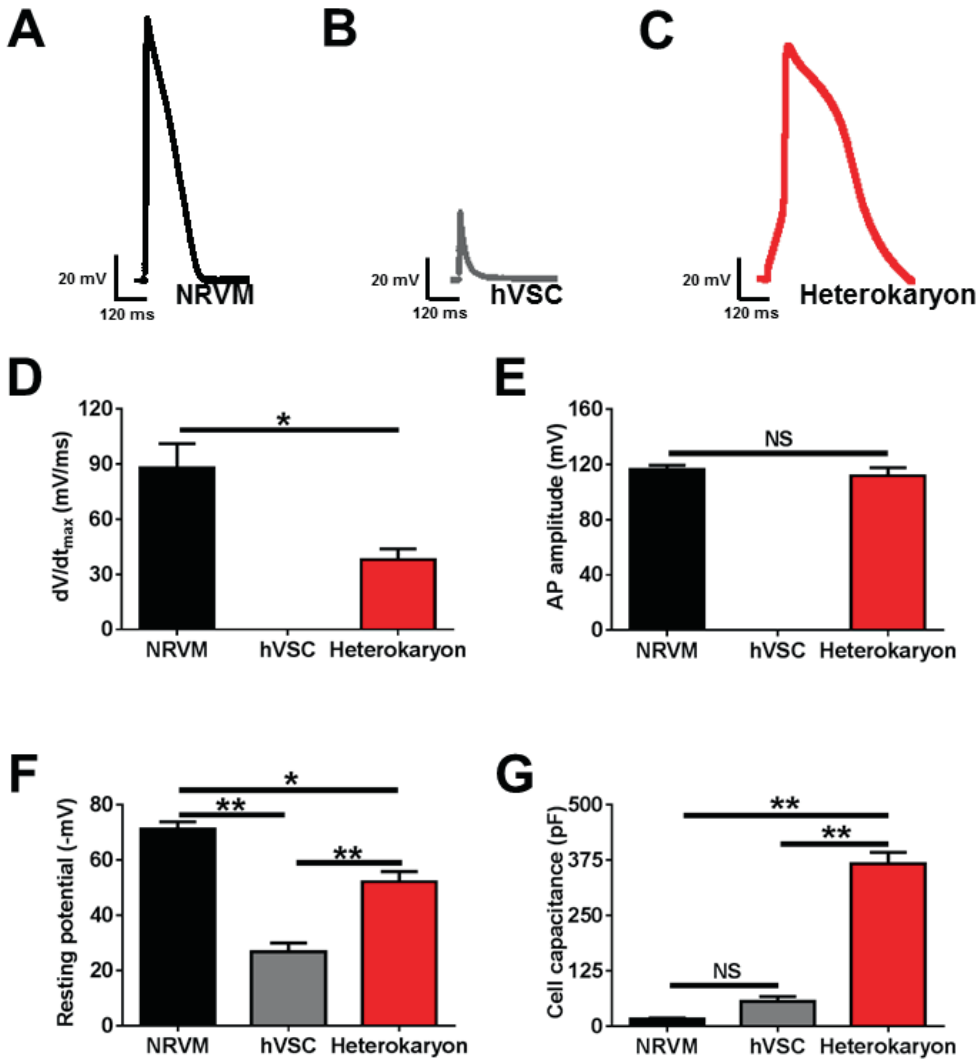

Figure 3. Fusion of hVSCs with NRVMs yields excitable heterokaryons. Typical current-clamp responses evoked by short current pulses in a single (*A*) NRVM, (*B*) hVSC and (*C*) responsive heterokaryon. Measurements from single NRVMs (N=8), single hVSCs (N=9) and isolated heterokaryons (N=9), comparing (*D*) maximum upstroke velocity (dV/dt_{max}), (*E*) AP amplitude and (*F*) resting membrane potential (RMP). To standardize the AP recording conditions, the cells were kept at a RMP of -80 mV by an appropriate holding current (*G*) C_m of isolated NRVMs, solitary hVSCs and isolated responsive and non-responsive heterokaryons.

Forced heterocellular fusion reduces arrhythmogenicity

To study the effects of heterocellular fusion in our fibrosis model, optical voltage mapping recordings were performed. Low pH-pretreated eGFP↑- and VSV-G/eGFP↑-co-cultures both showed convex 1:1 electrical propagation upon 1-Hz electrical stimulation (*Figure 4A*). However, EAD incidence in fused VSV-G/eGFP↑-co-cultures was much lower than in eGFP↑-co-cultures and similar to the EAD incidence in control NRVM cultures (*Figure 4B-D*). Furthermore, as compared to eGFP↑-co-cultures, fused VSV-G/eGFP↑-co-cultures displayed shorter APs, less APD dispersion and higher CVs (*Figure 4E-J*). Similar results were obtained for (co-)cultures subjected to 2-Hz electrical pacing. Patch-clamp experiments in monolayer cultures confirmed the beneficial effects of NRVM-hVSC fusion on APD, maximal upstroke velocity, AP amplitude and MDP (Supplementary material, *Figure S5*). Collectively, these data show that fusion of CMCs with hVSCs strongly reduces the arrhythmogenicity of fibrotic NRVM cultures.

Changes in cytosolic Ca^{2+} handling could be a possible mechanism contributing to the arrhythmogenic effect of fibrosis and of the beneficial effect of fibroblast-cardiomyocyte fusion in our co-cultures. To investigate this possibility, optical mapping experiments with the Ca^{2+} indicator Rhod-2-AM were carried out in NRVM cultures as non-fibrotic control cultures, eGFP↑-co-cultures and fused VSV-G/eGFP↑-co-cultures. For each culture type the duration of the Ca^{2+} waves (characterized by Ca^{2+} decay times) followed the APD (compare *Figure S6* with main manuscript, *Figure 4I*). This suggest that the arrhythmogenicity of unfused NRVM-hVSC co-cultures is not due to abnormalities in Ca^{2+} handling and that the beneficial effect of heterocellular fusion on fibrotic NRVM cultures does not result from the restoration of abnormalities in Ca^{2+}.

Heterokaryons show abundant expression of gap junctional proteins

Immunocytological staining of eGFP↑-co-cultures for connexin43 (Cx43) gave strong signals at CMC-CMC borders, but very weak signals at hVSC-CMC interfaces. In contrast, heterokaryons showed abundant Cx43 expression, predominantly at heterokaryon-CMC and heterokaryon-heterokaryon borders (*Figure 5A* and *B*). In line with these findings, mRNA levels for Cx43 were significantly higher in fused VSV-G/eGFP↑-co-cultures than in eGFP↑-co-cultures. Western blot analyses also showed protein levels of Cx43 to be significantly increased in fused as compared to non-fused NRVM-hVSC co-cultures (*Figure 5C*).

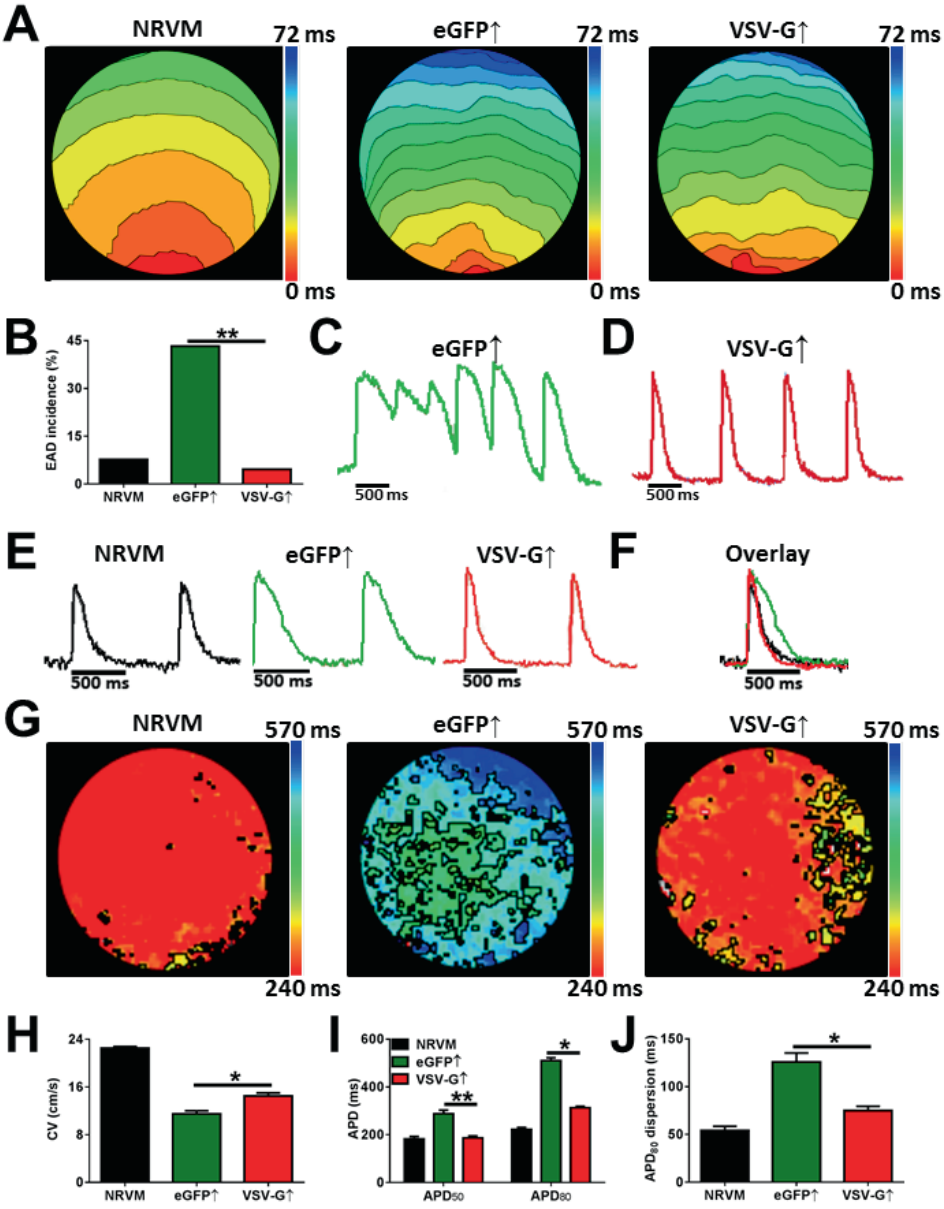

Figure 4. Heterocellular fusion reduces arrhythmogenicity in NRVM-hVSC co-cultures. Optical mapping of NRVM culture (NRVM; N=39), eGFP↑-co-cultures (eGFP↑; N=60), and fused VSV-G/eGFP↑-co-cultures (VSV-G↑; N=65). (*A*) Typical examples of activation maps (6-ms isochrone spacing) following 1-Hz pacing. (*B*) Quantification of EAD incidence. (*C*) Typical optical signal trace in an EAD-displaying eGFP↑-co-culture. (*D*) Typical optical signal trace in a fused, non-arrhythmic VSV-G/eGFP↑-co-culture. (*E*) Typical spatially and cubically filtered optical signal traces of NRVM culture (left), eGFP↑-co-culture (middle) and -VSV-G/eGFP↑-co-culture (right) following 1-Hz pacing, and (*F*) representative signal trace overlay. (*G*) Representative APD_{80} maps. Quantification of (*H*) CV, (*I*) APD_{50} and APD_{80}, and (*J*) APD_{80} dispersion.

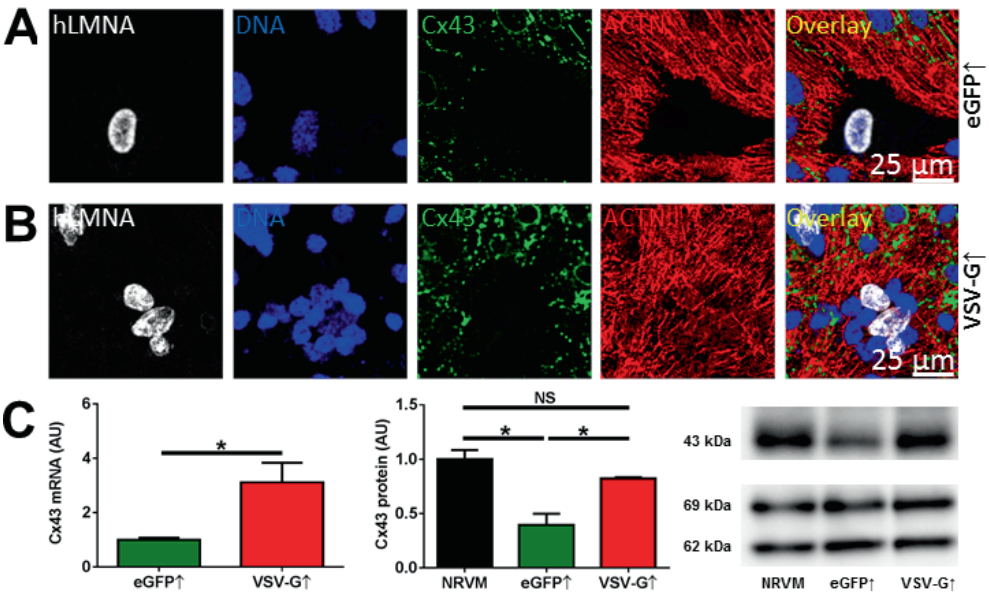

Figure 5. Heterocellular fusion increased gap junctional protein expression. Cells were stained for human lamin A/C (hLMNA, white), Hoechst 33342 (DNA, blue, nuclei), connexin43 (Cx43, green) and sarcomeric α-actinin (ACTN, red). (*A*) Representative eGFP↑-co-culture (eGFP↑) and (*B*) fused VSV-G/eGFP↑-co-culture (VSV-G↑). (*C*) Quantification of Cx43 mRNA (left panel) and protein (middle panel) and representative Western blot (right panel) showing the 43-kDa Cx43 protein as well lamin A/C protein species of 62 and 69 kDa, which served as loading controls. Quantitative data were based on 4 independent samples per group. AU, arbitrary units. Scale bar=25 μm.

Heterocellular fusion is anti-arrhythmic, at least partly, by enhancing repolarization force

Voltage-clamp analysis of the ionic membrane currents in single NRVMs, hVSCs and heterokaryons (Supplementary material, *Figure S7* and *Figure 6A*) showed that the NRVMs and hVSCs share their currents in the heterokaryons to a variable degree, causing about half of the heterokaryons to readily produce APs upon stimulation. Significant in this analysis was the increased I_{Kv} when averaged over its time course in the total pool of heterokaryons (Figure S7H), which resulted from an overall slower inactivation rate (Figure 6A-C). This I_{Kv} was strongly reduced by 40 mM TEA (Figure 6D-E). This observation allowed us to investigate whether the anti-arrhythmic effects of forced heterocellular fusion are mechanistically linked to the observed increase in repolarization force by optical mapping experiments on low pH-pretreated monolayer cultures after incubation of the cells with 40 mM TEA to block outward K_v currents. Both TEA-treated eGFP↑- and VSV-G/eGFP↑-co-cultures showed 1:1 electrical convex propagation from the pacing electrode upon 1-Hz pacing (*Figure 7A*). TEA treatment had no significant effect on CV (*Figure 7B*), but significantly increased APD_{80} and APD dispersion (*Figure 7C-F*). TEA treatment also significantly raised EAD incidence in VSV-G/eGFP↑-co-cultures, but not in eGFP↑-co-cultures where incidence was already high (*Figure 7G* and

H). On the other hand, exposure to 1 mM 4-AP, which inhibits average I_{Kv} by only ~30% (see Supplemental material), did not increase EAD incidence in fused VSV-G/eGFP↑-co-cultures, despite its prolonging effect on APD_{30} (Supplementary material, *Figure S8*). Collectively, these data demonstrate that upon TEA incubation, fused VSV-G/eGFP↑-co-cultures displayed a similar electrophysiological phenotype as unfused eGFP↑-co-cultures, in terms of APD, APD dispersion and EAD incidence. This strongly suggests that heterocellular fusion reduces the arrhythmogenicity of NRVM-hVSC co-cultures, at least partly, by enhancing repolarization force, consistent with the increased I_{Kv} found in the heterokaryons.

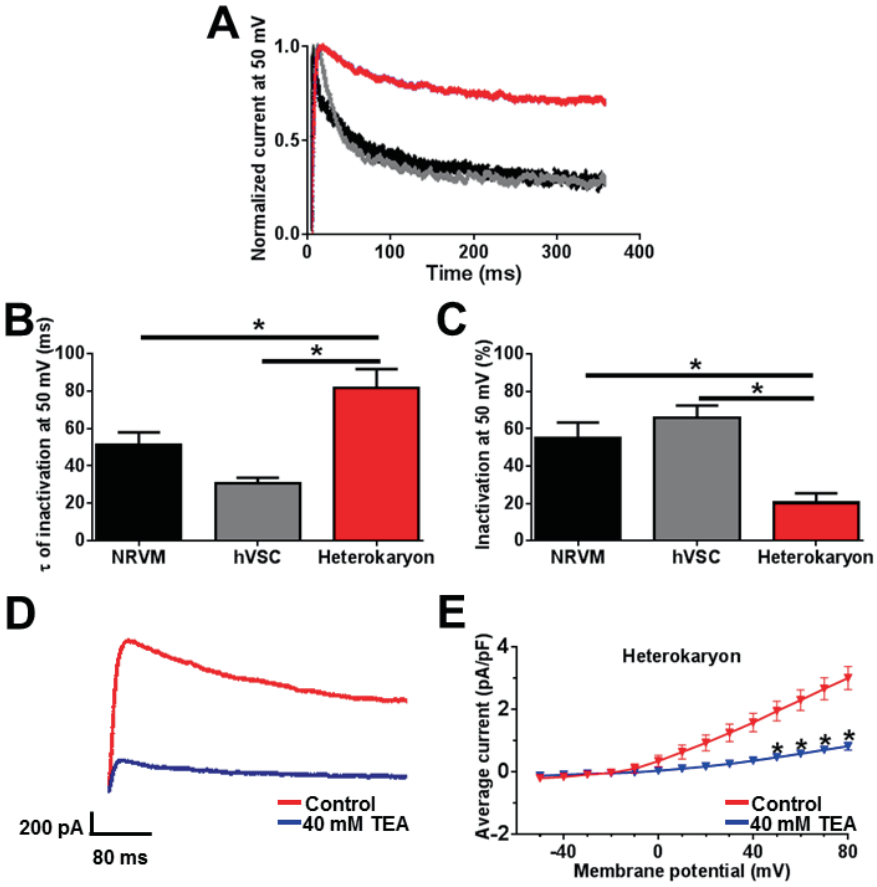

Figure 6. Heterokaryons possess outward K_v currents with slower inactivation kinetics than NRVMs or hVSCs and are TEA sensitive. (*A*) Typical outward current traces of the three cell types at 50 mV test potential, normalized for the initial peak amplitude. (*B*) Quantification of inactivation time constant (τ_{inact}) at 50 mV test potential. (*C*) Quantification of degree of current inactivation (I_{inact}) at 50 mV. (*D*) Superimposed typical records of whole-cell outward currents evoked at a test potential of 50 mV of a control (red) and TEA-treated (blue) heterokaryon. (*E*) Average current density-voltage plot of control (red) and TEA-treated (blue) heterokaryons shows a significant TEA-dependent decrease in current density at positive potentials.

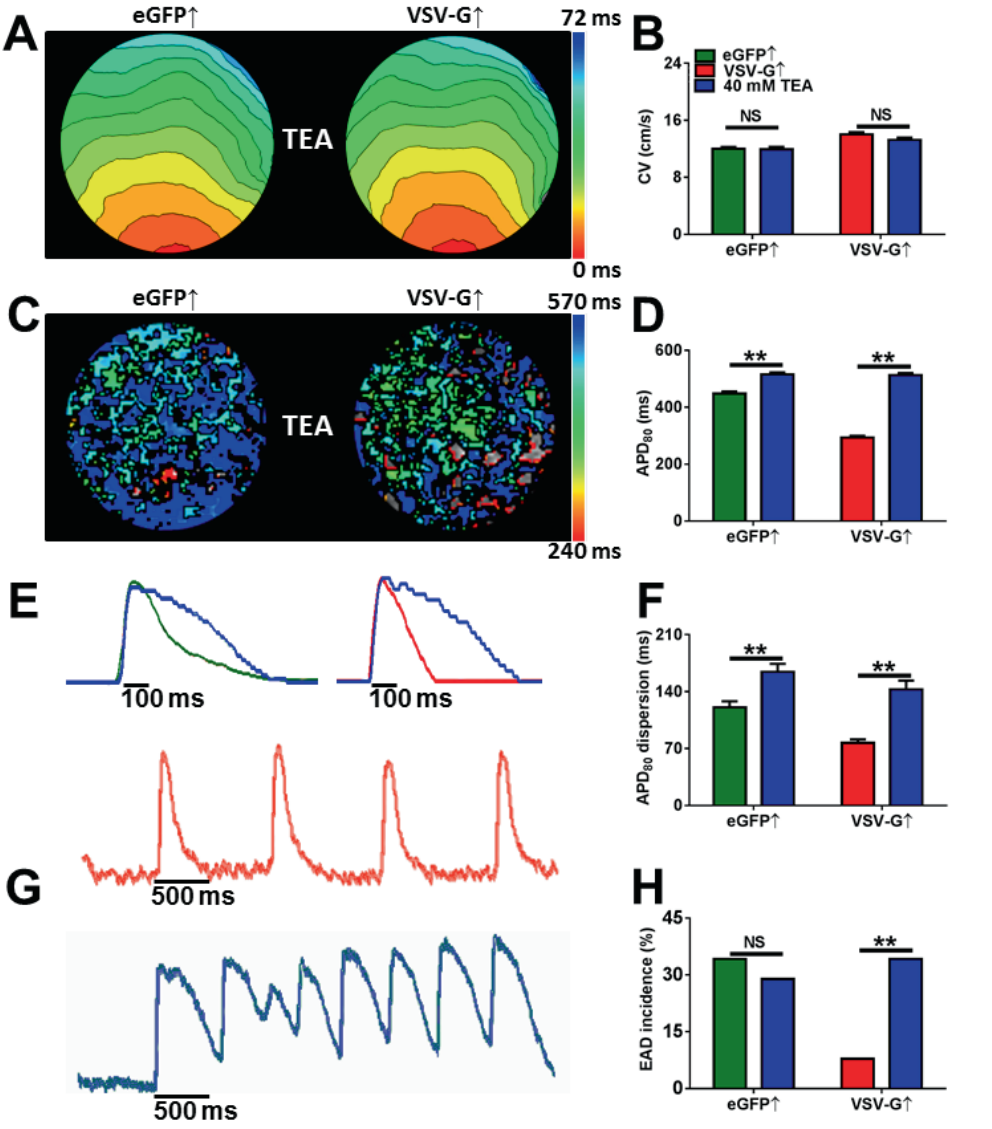

Figure 7. Inhibition of outward K_v currents abolishes the anti-arrhythmic effects of heterocellular fusion in VSVG/eGFP↑-co-cultures. (*A*) Typical activation maps (6-ms isochrone spacing) of TEA-treated eGFP↑-co-cultures (eGFP↑) and fused VSV-G/eGFP↑-co-cultures (VSV-G↑). (*B*) Quantification of CV in TEA-treated and control eGFP↑-co-cultures (N=38) and VSV-G/eGFP↑-co-cultures (N=38). (*C*) Typical APD_{80} maps of TEA-treated eGFP↑- and VSV-G/eGFP↑-co-cultures. (*D*) Effect of TEA on APD_{80}. (*E*) Typical spatially and cubically filtered optical signal trace overlays of a representative eGFP↑-co-culture (left) before (green) and after (blue) treatment with 40 mM TEA, and of a VSV-G/eGFP↑-co-culture (right) before (red) and after (blue) TEA treatment. (*F*) Effect of TEA on APD_{80} dispersion. (*G*) Typical spatially and cubically filtered optical signal traces of a representative VSV-G/eGFP↑-co-culture before (red) and after incubation with 40 mM TEA (blue). The blue signal trace shows the occurrence of multiple EADs. (*H*) Effect of TEA on EAD incidence.

Discussion

The key findings of this study are as follows: first, co-culture of hVSCs with NRVMs creates a pro-arrhythmic substrate by favoring EAD generation. Second, transduction of hVSCs with an LV encoding the fusogenic VSV-G endows these cells with controllable membrane fusion capacity, which enables them to fuse with surrounding NRVMs, resulting in formation of functional heterokaryons expressing high levels of Cx43 and showing strong outward K_v currents. Third, such forced cellular fusion of hVSCs with NRVMs reduces arrhythmogenicity in NRVM-hVSC co-cultures by preventing EADs. Finally, enhanced repolarization force is an important contributor to this anti-arrhythmic effect of heterocellular fusion.

Electrophysiological consequences of fibrosis

Intercellular communication between adjacent CMCs via gap junctions enables cardiac tissue to act as a functional syncytium and to ensure well-coordinated electrical and mechanical activation of the heart. In cardiac fibrosis, excessive deposition of extracellular matrix and local accumulation of inexcitable fibroblasts leads to disruptions of this syncytium.[6] While *in vitro* models to specifically study the role of the extracellular matrix on arrhythmogenesis remain to be developed, cell culture models have provided detailed information on the potential pro-arrhythmic effects of fibroblast-CMC interactions.[5,10] Consistent with these studies, our NRVM-hVSC co-cultures were slightly depolarized due to the (weak) electrical coupling of NRVMs to hVSCs.[22] This slight depolarization and the consequential increases in Na_v and K_v channel inactivation could at least partly explain the lower CV, longer APD and slower repolarization in the UT-co-cultures compared with the NRVM cultures. However, electrical coupling of the inexcitable hVSCs to the surrounding NRVMs could also have contributed to the lower CV and increased APD in the fibrotic NRVM cultures, due to the resulting capacitive loading of the NRVMs and its prolonging effect on both depolarization and repolarization time. Finally, a decrease in contact area between NRVMs due to insertion of hVSCs in between NRVMs, resulting in less efficient electric coupling between CMCs, may also have reduced CV. Besides a lower CV, the slower repolarization rate (causing "triangulation" of the AP) in the $I_{Ca,L}$ window current region seems another important cause of the high arrhythmogenicity of the NRVM-hVSC co-cultures as it favours EADs.[23] Previous studies demonstrated that paracrine factors released by CFBs change the electrophysiological properties of CMCs.[24,25] Transwell experiments showed that paracrine signaling from hVSCs did not have arrhythmogenic effects in our co-culture model. These disparate results may be explained by the fact that these previous studies were either carried out with CMCs and CFBs of neonatal rats or with CMCs and CFBs of adult rats using cell ratios and time points of assessment different from ours.[24,25] Paracrine signaling by CFBs could, however, still modulate other processes in CMCs, which were not investigated in this study.

Electrophysiological consequences of heterocellular fusion

Forced cellular fusion of hVSCs with NRVMs in NRVM-hVSC co-cultures resulted in an increase in CV, decreases in APD and APD dispersion, and, ultimately, in a lower EAD incidence. Heterokaryons resulting from NRVM-hVSC fusion seem to primarily owe their negative MDP to I_{Kir} and their excitability to I_{Nav} and $I_{Ca,L}$ of the NRVMs incorporated into the heterokaryons. The overall excitability of the responsive heterokaryons was, however, lower than that of NRVMs due to the decreased $I_{Ca,L}$ density and increased C_m. Apparently, the decreased I_{Kir} density in individual heterokaryons was still strong enough to bring the MDP to a value between those of single hVSCs and NRVMs, which was favoured by the small leakage conductance in heterokaryons. However, the MDP of fused VSV-G/eGFP↑-co-cultures did not significantly differ from that of NRVM cultures indicating that in our confluent monolayer cultures the heterokaryons were hyperpolarized by coupling with surrounding CMCs. Gap junctional coupling efficiency may be increased with heterocellular fusion considering the fusion-dependent increases in Cx43 transcript levels as well as in Cx43 protein levels and the abundant Cx43 expression at interfaces between adjacent heterokaryons and at borders between heterokaryons and NRVMs. In a previous study our research group showed that in confluent monolayer cultures hVSCs are electrically coupled with surrounding NRVMs albeit weakly,[10] which corresponds to the low Cx43 expression at hVSC-NRVM interfaces in the eGFP↑-co-cultures. Efficient electrical coupling of heterokaryons with surrounding non-fused NRVMs may explain why cardiac excitation waves are well conducted through heterokaryons, despite their reduced excitability in comparison to NRVMs. Efficient gap junctional coupling is also expected to increase CV by lowering intercellular resistance. An additional possible reason for the increase in CV in fibrotic NRVM cultures after fusion could be the presence of enlarged intracellular compartments allowing APs to traverse several NRVM diameters at once.

Another important aspect is the significant role for repolarizing currents in the anti-arrhythmic effects of forced heterocellular fusion, as indicated by patch-clamp measurements. After compensation for cell size, a significantly stronger transient outward K_v current with slower inactivation kinetics was observed in heterokaryons than in NRVMs. The resulting increase in repolarization force could explain the observed reduction of APD and EAD incidence. This notion was confirmed by our TEA experiments, which showed that I_{Kv} inhibition in fused VSV-G/eGFP↑-co-cultures resulted in loss of the anti-arrhythmic effects of heterocellular fusion as manifested by an increase in EAD incidence to a value similar to that of non-fused NRVM-hVSC co-cultures. The exact mechanisms by which forced heterocellular fusion between hVSCs and NRVMs increases the outward K_v currents in fusion products warrants further investigation. One possibility is selective activation of K_v channel genes as a result of the fusion process due to the combinatorial effects of transcriptional regulators from two different cell types. Depending on

the specific epigenetic landscapes in the nuclei of NRVMs and hVSCs, transcription of certain genes may be more readily upregulated in heterokaryons than that of others. If there was a selection for K_v channels, this could have accounted for the enhanced K_v current seen after fusion. The mixed content of NRVMs and hVSCs in heterokaryons could also have increased the activity of individual K_v channels by altered posttranslational modifications or association with other regulatory proteins. The strong Cx43 expression at heterokaryon-CMC interfaces might also allow heterokaryonic I_{Kv} to facilitate repolarization of surrounding NRVMs and I_{Kir} from NRVMs to support repolarization of adjacent heterokaryons. This mutual sharing of two repolarizing channel types may cause an overall faster repolarization and, consequently, less AP triangulation. This, in turn, would have an anti-arrhythmic effect by reducing EAD risk.[23] However, furthering our understanding on the precise role of electrical coupling in cardiac impulse propagation after heterocellular fusion will depend on dedicated studies. These studies should also address to what extent heterokaryons are able to respond to subsequent pathological processes by gap junctional modulation, like normally occurs in damaged myocardium to prevent spread of death signals to surrounding healthy cardiac tissue.[26]

Regarding the effect of heterocellular fusion on Ca^{2+} handling, our patch-clamp data show that the average Ca^{2+} peak current in heterokaryons is decreased compared with NRVMs, while Ca^{2+} transient decay times are smaller in fused VSV-G/eGFP-↑-co-cultures than in eGFP↑-co-cultures. The underlying molecular mechanisms of these findings warrant further investigation, but previous studies have shown that decreases in $I_{Ca,L}$ and Ca^{2+} transient decay time are associated with a reduction in EAD incidence.[27] In our co-culture model, repolarizing K^+ currents and opposing Ca^{2+} currents seem to be the main determinants of EAD risk. Previously, APD prolongation associated with K^+ current downregulation was shown to be important in generating the $I_{Ca,L}$-mediated component of EADs.[28] This is in agreement with our data, since inhibition of I_{Kv} in fused VSV-G/eGFP-↑-co-cultures by TEA completely annulled the suppressive effect of heterocellular fusion on EAD incidence in fibrotic NRVM cultures.

However, it is likely that additional mechanisms add to the anti-arrhythmic effects of forced heterocellular fusion. For example, cell-to-cell fusion increases C_m, which impacts electrophysiological source-sink relationships and thereby reduces the likelihood of EAD propagation.[29] As the anti-arrhythmic effects of forced heterocellular fusion seems to be the resultant of multiple interacting factors, future studies should be directed at unraveling the individual contributions of each of them. For instance, *in silico* experiments could show the effect of selective downregulation of K_v currents (I_{Ks}, I_{Kr}) and thereby clarify their individual roles in increasing repolarization force and decreasing EAD incidence. Similarly, modulation of gap junctional protein (especially Cx43) expression could give insight into the contribution of electrical coupling to the anti-arrhythmic effects of NRVM-hVSC fusion.

Taken together, the present study presents proof-of-concept of heterocellular fusion as a novel means to modify electrophysiological properties on a multicellular level. Our findings may also trigger the exploration of new treatment options for fibrosis-mediated arrhythmias aimed at increasing electrical homogeneity by heterocellular fusion or other means.

Clinical perspectives and study limitations

The extent and functional relevance of heterocellular coupling in healthy and diseased myocardium, especially between (myo)fibroblasts and adjacent CMCs, is still unclear. Dedicated transgenic animal models and specialized techniques are probably needed to unravel the role of CMC-CFB coupling in the intact heart as a prerequisite for translation of our results to the *in vivo* setting.[30] In fact, before heterocellular fusion could be considered as a possible therapeutic modality, several important issues need to be resolved. Whether heterocellular fusion is safe would have to be addressed first by investigating its effect on myocardial integrity, stiffness and contractility. Furthermore, although our results in the 2D co-culture model suggest an anti-arrhythmic effect of heterocellular fusion, it is uncertain whether the same holds true in the 3D myocardium, with its complex anatomy and its different, disease-specific patterns of fibrosis.[31] Since our model was limited to a diffuse pattern of fibrosis, the effects of heterocellular fusion on other types of cardiac fibrosis remain to be investigated. In addition, apart from lowering pro-arrhythmic risk by decreasing EAD incidence, the APD-shortening effect of heterocellular fusion in VSV-G/eGFP-↑-co-cultures may also increase arrhythmogenic potential as it increases the risk for reentrant circuit formation due to a decrease in wavelength.[32] Although we did not find any evidence of reentrant tachyarrhythmias in our model, whether the same is true *in vivo* remains to be studied.

Regarding the limitations of our model, CMCs from neonatal rats were used since human CMCs could not be obtained in amounts sufficient for the experiments with monolayers presented in this study. Although these monolayers provide a standardized and controllable 2D model of fibrosis-related arrhythmias, these disorders normally occur in the 3D myocardium of diseased hearts. Nevertheless, 2D models with NRVMs have proven their usefulness as a model system for studying key electrophysiological processes of the heart.[33] Furthermore, while the beginning and duration of heterocellular fusion could be tightly controlled by timed exposure of the VSV-G/eGFP-↑-co-cultures to low pH medium, the quantitative aspects of fusion were less easy to control, but still allowed us to perform reproducible studies. This limitation resulted in heterokaryons of different composition and therefore with various degrees of excitability. Hence, it would be important for future studies to develop a fusion method with greater control over the final composition and electrical properties of the fusion products. Nonetheless, even with the current approach, a fusion-dependent decrease in arrhythmogenicity of fibrotic CMC cultures could be demonstrated.

Conclusions

In summary, forced cellular fusion of hVSCs with NRVMs in confluent monolayer cultures yields functional heterokaryons and reduces arrhythmogenicity by preventing the occurrence of EADs. This decrease in EAD incidence is, at least partly, attributable to an increase in repolarization force, but is also associated with increased intercellular Cx43 expression and reduced Ca^{2+} decay time. Forced heterocellular fusion could provide a novel basis for anti-arrhythmic engineering of cardiac tissue.

Funding

This work was supported by the Netherlands Organization for Scientific Research (NWO) [Mosaic grant 017007064 to M.C.E. and Veni grant 91611070 to D.A.P.], the Dutch Heart Foundation (2014T110 to S.F.A.A.), Ammodo (to D.A.P.) and by the Royal Netherlands Academy of Arts and Sciences (KNAW) [CEP project 10CDP007 to A.A.F.d.V.].

Acknowledgements

We thank our LUMC colleagues Margreet de Jong and Rebecca Feistritzer from the Laboratory of Experimental Cardiology for excellent technical support, Martin Jan Schalij for critically reading the manuscript, and Annelies van der Laan and Joop Wiegant from the Department of Molecular Cell Biology for technical assistance with confocal microscopy.

Conflict of interest

None declared.

References

1. Kakkar R, Lee RT. Intramyocardial fibroblast myocyte communication. *Circ Res.* 2010;106:47-57.
2. Souders CA, Bowers SL, Baudino TA. Cardiac fibroblast: the renaissance cell. *Circ Res.* 2009;105:1164-1176.
3. Leask A. Getting to the Heart of the Matter: New Insights Into Cardiac Fibrosis. *Circ Res.* 2015;116:1269-1276.
4. Sun Y, Weber KT. Infarct scar: a dynamic tissue. *Cardiovasc Res.* 2000;46:250-256.
5. Rohr S. Arrhythmogenic implications of fibroblast-myocyte interactions. *Circ Arrhythm Electrophysiol.* 2012;5:442-452.
6. Nguyen TP, Qu Z, Weiss JN. Cardiac fibrosis and arrhythmogenesis: the road to repair is paved with perils. *J Mol Cell Cardiol.* 2014;70:83-91.
7. Kohl P, Camelliti P, Burton FL, Smith GL. Electrical coupling of fibroblasts and myocytes: relevance for cardiac propagation. *J Electrocardiol.* 2005;38:45-50.
8. McDowell KS, Arevalo HJ, Maleckar MM, Trayanova NA. Susceptibility to arrhythmia in the infarcted heart depends on myofibroblast density. *Biophys J.* 2011;101:1307-1315.
9. Xie Y, Garfinkel A, Camelliti P, Kohl P, Weiss JN, Qu Z. Effects of fibroblast-myocyte coupling on cardiac conduction and vulnerability to reentry: A computational study. *Heart Rhythm.* 2009;6:1641-1649.
10. Pijnappels DA, van Tuyn J, de Vries AA, Grauss RW, van der Laarse A, Ypey DL, Atsma DE, Schalij MJ. Resynchronization of separated rat cardiomyocyte fields with genetically modified human ventricular scar fibroblasts. *Circulation.* 2007;116:2018-2028.
11. Cho HC, Marban E. Biological therapies for cardiac arrhythmias: can genes and cells replace drugs and devices? *Circ Res.* 2010;106:674-685.
12. Shiba Y, Fernandes S, Zhu WZ, Filice D, Muskheli V, Kim J, Palpant NJ, Gantz J, Moyes KW, Reinecke H, Van BB, Dardas T, Mignone JL, Izawa A, Hanna R, Viswanathan M, Gold JD, Kotlikoff MI, Sarvazyan N, Kay MW, Murry CE, Laflamme MA. Human ES-cell-derived cardiomyocytes electrically couple and suppress arrhythmias in injured hearts. *Nature.* 2012;489:322-325.
13. Chong JJ, Yang X, Don CW, Minami E, Liu YW, Weyers JJ, Mahoney WM, Van BB, Cook SM, Palpant NJ, Gantz JA, Fugate JA, Muskheli V, Gough GM, Vogel KW, Astley CA, Hotchkiss CE, Baldessari A, Pabon L, Reinecke H, Gill EA, Nelson V, Kiem HP, Laflamme MA, Murry CE. Human embryonic-stem-cell-derived cardiomyocytes regenerate non-human primate hearts. *Nature.* 2014;510:273-277.
14. Kizana E, Ginn SL, Allen DG, Ross DL, Alexander IE. Fibroblasts can be genetically modified to produce excitable cells capable of electrical coupling. *Circulation.* 2005;111:394-398.
15. Ieda M, Fu JD, Delgado-Olguin P, Vedantham V, Hayashi Y, Bruneau BG, Srivastava D. Direct reprogramming of fibroblasts into functional cardiomyocytes by defined factors. *Cell.* 2010;142:375-386.
16. Chen JX, Krane M, Deutsch MA, Wang L, Rav-Acha M, Gregoire S, Engels MC, Rajarajan K, Karra R, Abel ED, Wu JC, Milan D, Wu SM. Inefficient reprogramming of fibroblasts into cardiomyocytes using Gata4, Mef2c, and Tbx5. *Circ Res.* 2012;111:50-55.
17. Gottesman A, Milazzo J, Lazebnik Y. V-fusion: a convenient, nontoxic method for cell fusion. *Biotechniques.* 2010;49:747-750.
18. van Tuyn J, Pijnappels DA, de Vries AA, de V, I, van der Velde-van Dijke, Knaan-Shanzer S, van der Laarse A, Schalij MJ, Atsma DE. Fibroblasts from human postmyocardial infarction scars acquire properties of cardiomyocytes after transduction with a recombinant myocardin gene. *FASEB J.* 2007;21:3369-3379.
19. Askar SF, Ramkisoensing AA, Schalij MJ, Bingen BO, Swildens J, van der Laarse A, Atsma DE, de Vries AA, Ypey DL, Pijnappels DA. Antiproliferative treatment of myofibroblasts prevents arrhythmias in vitro by limiting myofibroblast-induced depolarization. *Cardiovasc Res.* 2011;90:295-304.

20. Askar SF, Ramkisoensing AA, Atsma DE, Schalij MJ, de Vries AA, Pijnappels DA. Engraftment patterns of human adult mesenchymal stem cells expose electrotonic and paracrine proarrhythmic mechanisms in myocardial cell cultures. *Circ Arrhythm Electrophysiol.* 2013;6:380-391.

21. Bingen BO, Engels MC, Schalij MJ, Jangsangthong W, Neshati Z, Feola I, Ypey DL, Askar SF, Panfilov AV, Pijnappels DA, de Vries AA. Light-induced termination of spiral wave arrhythmias by optogenetic engineering of atrial cardiomyocytes. *Cardiovasc Res.* 2014;104:194-205.

22. Jacquemet V, Henriquez CS. Loading effect of fibroblast-myocyte coupling on resting potential, impulse propagation, and repolarization: insights from a microstructure model. *Am J Physiol Heart Circ Physiol.* 2008;294:H2040-H2052.

23. Weiss JN, Garfinkel A, Karagueuzian HS, Chen PS, Qu Z. Early afterdepolarizations and cardiac arrhythmias. *Heart Rhythm.* 2010;7:1891-1899.

24. Pedrotty DM, Klinger RY, Kirkton RD, Bursac N. Cardiac fibroblast paracrine factors alter impulse conduction and ion channel expression of neonatal rat cardiomyocytes. *Cardiovasc Res.* 2009;83:688-697.

25. Cartledge JE, Kane C, Dias P, Tesfom M, Clarke L, Mckee B, Al AS, Chester A, Yacoub MH, Camelliti P, Terracciano CM. Functional crosstalk between cardiac fibroblasts and adult cardiomyocytes by soluble mediators. *Cardiovasc Res.* 2015;105:260-270.

26. Garcia-Dorado D, Rodriguez-Sinovas A, Ruiz-Meana M. Gap junction-mediated spread of cell injury and death during myocardial ischemia-reperfusion. *Cardiovasc Res.* 2004;61:386-401.

27. January CT, Riddle JM. Early afterdepolarizations: mechanism of induction and block. A role for L-type Ca2+ current. *Circ Res.* 1989;64:977-990.

28. Zeng J, Rudy Y. Early afterdepolarizations in cardiac myocytes: mechanism and rate dependence. *Biophys J.* 1995;68:949-964.

29. Xie Y, Sato D, Garfinkel A, Qu Z, Weiss JN. So little source, so much sink: requirements for afterdepolarizations to propagate in tissue. *Biophys J.* 2010;99:1408-1415.

30. Quinn TA, Camelliti P, Siedlecka U, Poggioli T, Loew LM, Knöpfel T, Kohl P. Cell-specific expression of voltage-sensitive protein confirms cardiac myocyte to non-myocyte electrotonic coupling in healed murine infarct border tissue. *Circulation* 2014;130:A11749.

31. de Jong S, van Veen TA, van Rijen HV, de Bakker JM. Fibrosis and cardiac arrhythmias. *J Cardiovasc Pharmacol.* 2011;57:630-638.

32. Kleber AG, Rudy Y. Basic mechanisms of cardiac impulse propagation and associated arrhythmias. *Physiol Rev.* 2004;84:431-488.

33. Herron TJ, Lee P, Jalife J. Optical imaging of voltage and calcium in cardiac cells & tissues. *Circ Res.* 2012;110:609-623.

Supporting information

Methods

Animal studies

All animal experiments were approved by the Animal Experiments Committee of the Leiden University Medical Center (LUMC) and conformed to the Guide for the Care and Use of Laboratory Animals as stated by the US National Institutes of Health.

Human ventricular scar cell (hVSC) isolation and culture

Human tissue was collected in accordance with guidelines posed by the Medical Ethics Committee of the LUMC and adhered to the principles described in the Declaration of Helsinki. hVSCs were isolated as described previously.[1,2] Surgical waste material consisting of human myocardial scar tissue was obtained from 10 patients undergoing left ventricle reconstructive surgery (Dor procedure). Samples were cut into small pieces (1-3 mm diameter), transferred to 6-well cell culture plates (Corning Life Sciences, Corning, NY) coated with porcine gelatin (Sigma-Aldrich, St. Louis, MO) and covered with round glass coverslips (30 mm in diameter) to prevent floating. Cells were cultured in a humidified 95% air/5% CO_2 environment at 37°C. hVSC culture medium, consisting of Dulbecco's modified Eagle's medium (DMEM; Life Technologies, Bleiswijk, the Netherlands) containing 10% fetal bovine serum (FBS), 100 U/mL penicillin, 100 µg/mL streptomycin, 2 mM GlutaMAX-I and 1 mM sodium pyruvate (all from Life Technologies), was refreshed every 3 days. The cells that grew out of the tissue pieces were trypsinized (0.05% trypsin-EDTA; Life Technologies), frozen in FBS/10% dimethyl sulfoxide (DMSO; Miltenyi Biotec, Leiden, the Netherlands) and stored in the vapor compartment of a liquid nitrogen tank at -175° C until use. Cells at passage numbers 2-4 were used for further experiments.

Construction of self-inactivating lentiviral vector (SIN-LV) shuttle plasmids

Plasmid construction was performed using standard techniques or following the instructions accompanying specific reagents.[3] The construction of the monocistronic enhanced green fluorescent protein (eGFP)-encoding SIN-LV shuttle plasmid pLV.hCMV-IE.IRES.eGFP.hHBVPRE (main manuscript, *Figure 2A*) has been described elsewhere.[4] The bicistronic SIN-LV shuttle plasmid pLV.hCMV-IE.VSV-G.IRES.eGFP.hHBVPRE (main manuscript, *Figure 2B*), which codes for eGFP and for the vesicular stomatitis virus G (VSV-G) protein, was generated by insertion of the 1.7-kb EcoRI fragment of pLP.VSV-G (Life Technologies) in the proper orientation in between the two EcoRI recognition sites of pLV.hCMV-IE.IRES.eGFP.hHBVPRE. The correctness of pLV.hCMV-IE.VSV-G.IRES.eGFP.hHBVPRE was verified by restriction mapping using 5 different enzymes. Restriction endonucleases and other DNA modifying enzymes were obtained from Thermo Fisher Scientific (Landsmeer, the Netherlands) or New England Biolabs (Bioké, Leiden,

the Netherlands). For large-scale purification of the SIN-LV shuttle and packaging plasmids the JETSTAR 2.0 Plasmid Maxiprep kit (Genomed, Löhne, Germany) was used following the instructions of the manufacturer.

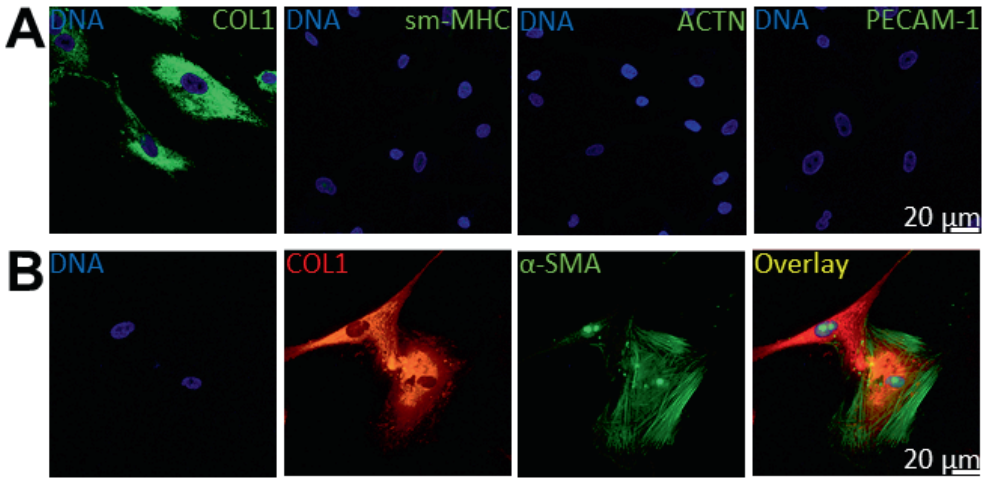

Supplementary Figure S1. Immunocytological characterization of hVSCs. (*A*) Cells were immunostained for collagen type I (COL1, green, fibroblastic cells), smooth muscle myosin heavy chain (sm-MHC, green, smooth muscle cells), sarcomeric α-actinin (ACTN, green, cardiomyocytes), CD31 (PECAM-1, green, endothelial cells) and Hoechst 33342 (DNA, blue, nuclei). (*B*) hVSCs were immunostained for collagen type I (COL1, red, fibroblastic cells) and α-smooth muscle actin (α-SMA, green, myofibroblastic cells and smooth muscle cells). Quantifications wre based on 3 independent isolations and 25 images.

The abbreviations used in *Figure 2A* and *B* of the main manuscript are explained as follows: 5′ LTR: chimeric 5′ long terminal repeat containing enhancer and promoter elements of Rous sarcoma virus and the human immunodeficiency virus type 1 (HIV1) R and U5 regions. Ψ: HIV1 packaging signal. RRE: HIV1 Rev-responsive element. cPPT: HIV1 central polypurine tract and termination site. hCMV-IE: human cytomegalovirus *immediate early* promotor. VSV-G: vesicular stomatitis virus glycoprotein-coding sequence. EMCV IRES: encephalomyocarditis virus internal ribosome entry site. eGFP: *Aequorea victoria* enhanced green fluorescent protein-encoding sequence. hHBVPRE: human hepatitis B virus posttranscriptional regulatory element. 3′: wildtype 3′ HIV1 long terminal repeat with a large deletion in the U3 region.

SIN-LV production and transduction

LV.VSV-G/eGFP↑ and LV.eGFP↑ particles were produced in 293T cells from SIN-LV shuttle plasmids pLV.hCMV-IE.VSV-G.IRES.eGFP.hHBVPRE and pLV.hCMV-IE.IRES.eGFP.hHBVPRE, respectively, as described previously.[5] SIN-LV particles were concentrated by ultracentrifugation and subsequently suspended in phosphate-buffered saline (PBS) containing 1% bovine serum albumin (BSA) fraction V (Sigma-Aldrich). SIN-LV suspensions were stored in 100 µL portions at

-80°C until use. hVSCs were thawed freshly for each experiment 4 days before co-culture. At 1 day after culture initiation, hVSCs were transduced by adding SIN-LV suspension directly to culture medium containing 10 µg/mL diethylaminoethyl-dextran (Carl Roth, Karlsruhe, Germany). At 24 h after vector addition, the inoculum was removed. LV.VSV-G/eGFP↑-transduced hVSCs (hereinafter referred to as VSV-G/eGFP↑-hVSCs) and LV.eGFP↑-transduced hVSCs (hereinafter referred to as eGFP↑-hVSCs) were then washed 3 times with culture medium and kept in fresh culture medium for 2 additional days until establishment of co-cultures with neonatal rat ventricular myocytes (NRVMs). Transduction efficiency was determined by assessment of eGFP fluorescence with an Axiovert 200M inverse fluorescence microscope (Carl Zeiss, Sliedrecht, the Netherlands). SIN-LVs were applied at doses that resulted in transduction of nearly 100% of hVSCs, without microscopic signs of cytotoxicity.

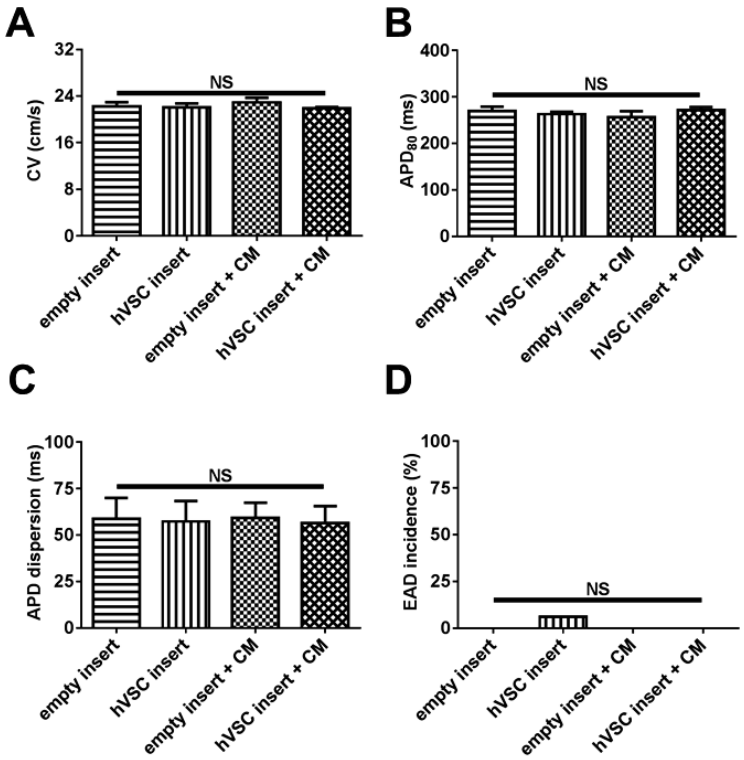

Supplementary Figure S2. Investigation of the effects of paracrine factors released by hVSCs on the electrophysiological behavior of NRVMs using transwell assay and optical voltage mapping. NRVM cultures incubated with empty transwell inserts (empty insert; N=8), NRVM cultures incubated with hVSC-containing transwell inserts (hVSC insert; N=16), NRVM cultures incubated with empty inserts and conditioned hVSC medium (empty insert + CM; N=8) and NRVM cultures incubated with hVSC-containing inserts and conditioned medium (hVSC insert + CM; N=16) were analyzed for (*A*) CV, (*B*) APD_{80}, (*C*) APD_{80} dispersion and (*D*) EAD incidence.

Neonatal rat ventricular cardiomyocyte (NRVM) isolation and co-culture

NRVMs were isolated as described previously.[6] Briefly, neonatal Wistar rats (2 days *post-partum*) were anaesthetized by 5% isoflurane inhalation and adequate anaesthesia was confirmed by absence of reflexes. Hearts were rapidly excised and after removal of atrial tissue, the ventricles were finely minced and dissociated with collagenase type 1 (450 U/mL; Worthington, Lakewood, NJ) and DNase I (18.75 Kunitz/mL; Sigma-Aldrich). The resulting cell suspension was applied to Primaria cell culture dishes (BD Biosciences, Breda, the Netherlands) and incubated for 75 min at 37°C and 5% CO_2 to allow preferential attachment of non-myocytes (predominantly cardiac fibroblasts). Unattached cardiac cells (mainly NRVMs) were passed through a cell strainer (70 µm mesh pore size; BD Biosciences), to obtain a single cell suspension, and seeded in 24-well cell culture plates (Corning Life Sciences) onto bovine fibronectin (Sigma-Aldrich) -coated round glass coverslips (15 mm in diameter). For establishing NRVM-hVSC co-cultures, hVSCs were trypsinized and counted on the day of NRVM isolation and mixed with the NRVMs in a ratio of 4 NRVMs:1 hVSC before plating. Co-cultures were established with untransduced hVSCs (UT-co-cultures), eGFP↑-hVSCs (eGFP↑-co-cultures) or VSV-G/eGFP↑-hVSCs (VSV-G/eGFP↑-co-cultures). Cells were plated at a total density of 0.5-6×10^5 cells/well, depending on the assay. At day 1 of culture, cells were incubated with mitomycin-C (10 µg/mL; Sigma-Aldrich) for 2 h to inhibit cell proliferation, as described previously.[7] Culture medium (hereinafter referred to as NRVM culture medium) consisted of DMEM/Ham's F10 medium (1:1, v/v; Life Technologies) supplemented with 5% horse serum (Life Technologies), 2% BSA and sodium ascorbate to a final concentration of 0.4 mM and was refreshed daily.

Immunocytology

Cells were fixed with PBS/4% formaldehyde (Merck, Amsterdam, the Netherlands) for 15 min at room temperature (RT), washed 3 times with PBS and permeabilized by incubation for 10 min at RT with PBS/0.05% Triton-X100 (Sigma-Aldrich). After 3 washes with PBS/0.1% Tween-20 (Sigma-Aldrich), samples were incubated with primary antibodies diluted in PBS/10% FBS/1% BSA. Antibodies against the following antigens were used: human lamin A/C to detect cells of human origin (1:200; mouse IgG2b, clone 636; Vector Laboratories, Burlingame, CA), sarcomeric α-actinin to detect NRVMs (1:300; mouse IgG1, clone EA-53; Sigma-Aldrich), collagen type 1 to identify fibroblastic cell types (1:300; rabbit IgG, polyclonal; Abcam, Cambridge, United Kingdom), smooth muscle myosin heavy chain (MYH11 gene product) to detect smooth muscle cells (1:200; mouse IgG1, clone hSM-V; Sigma-Aldrich), CD31 (PECAM-1 gene product) to identify endothelial cells (1:200; rat IgG2a, clone MEC 13.3; BD Biosciences), α-smooth muscle actin (ACTA2 gene product) to detect myofibroblasts and smooth muscle cells (1:200; mouse IgG2a, clone 1A4; Sigma-Aldrich), GFP to detect LV.eGFP↑- and LV.VSV-G/eGFP↑-transduced cells (1:200, rabbit IgG, polyclonal; Life Technologies), VSV-G to detect LV.VSV-G/

eGFP↑-transduced cells (1:200; mouse IgG1, clone P5D4, Cy3-conjugated; Sigma-Aldrich) and connexin43 (1:200; rabbit IgG, polyclonal; Sigma-Aldrich). After washing 3 times for 5 min with PBS/0.1% Tween-20, cells were incubated with appropriate Alexa Fluor 488/568-conjugated secondary antibodies (1:500; Life Technologies) or, for detecting human lamin A/C, with biotin-conjugated goat-anti mouse IgG_{2b} secondary antibodies (1:200; Santa Cruz Biotechnology, Santa Cruz, CA) and Qdot 655 streptavidin conjugates (1:200; Life Technologies). The VSV-G protein was detected without the use of secondary antibodies due to the covalent linkage of the primary antibodies to Cy3. Nuclear counterstaining was performed by incubating the cells for 10 min at RT with 10 µg/mL Hoechst 33342 (Life Technologies). Coverslips were mounted in Vectashield mounting medium (Vector Laboratories). Images were acquired with a Leica TCS SP8 confocal laser scanning microscope (Leica Microsystems, Rijswijk, the Netherlands) or with a digital color camera-equipped fluorescence microscope (Nikon Eclipse 80i; Nikon Instruments Europe, Amstelveen, the Netherlands). Storage and quantification of immunofluorescence signals was done using dedicated software (Leica Application Suite [Leica Microsystems], NIS Elements [Nikon Instruments Europe] and Fiji [www.fiji.sc]). Each immunostaining was performed on at least 3 independent cell cultures.

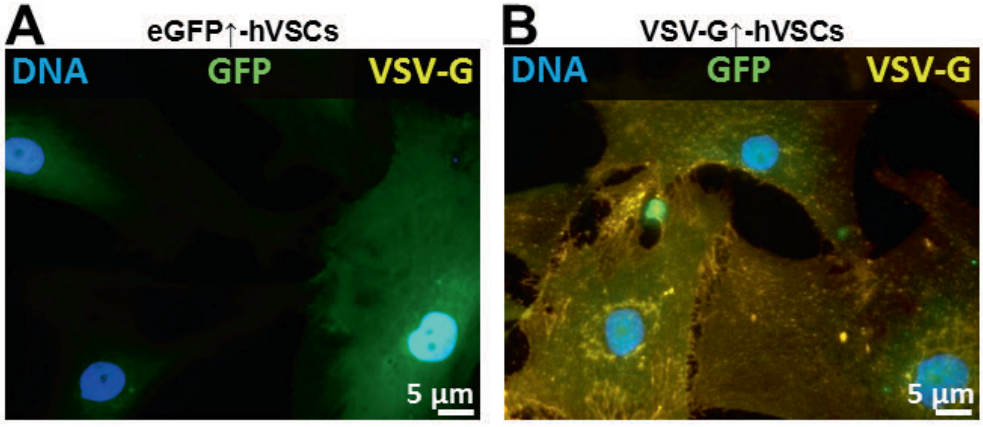

Supplementary Figure S3. Immunocytological confirmation of forced VSV-G expression following transduction of hVSCs with LV.VSV-G/eGFP↑. Immunocytological staining of hVSC monocultures consisting of (*A*) eGFP↑-hVSCs and (*B*) VSV-G/eGFP↑-hVSCs for green fluorescent protein (GFP; green), vesicular stomatitis virus G protein (VSV-G; yellow) and DNA (blue). $VSV\text{-}G^+$ cells were only present in the LV.VSV-G/eGFP↑-transduced hVSC cultures. Based on 3 independent transductions and 30 images.

Reverse transcription quantitative-polymerase chain reaction (RT-qPCR) analysis

Dedicated cell cultures samples were used for RT-qPCR experiments, which were performed as described previously.[8] Briefly, cells were lysed using TRIzol reagent (Life Technologies) and total RNA was isolated with the RNeasy Mini Kit (Qiagen, Venlo, the Netherlands). Reverse transcription was performed using the iScript cDNA synthesis kit (Bio-Rad Laboratories, Veenendaal, the Netherlands). Connexin43 (Cx43) mRNA expression levels were quantified with the Bioline SensiFAST SYBR No-ROX kit (Meridian Biosciences, Singapore), using oligodeoxyribonucleotides: 5′ GGGATAAGGGAGGTACACA 3′ (rat Gja1-specific forward primer) and 5′ CACTCAATTCATGTACACAGACT 3′ (rat Gja1-specific reverse primer). For normalisation purposes, 18S rRNA sequences were amplified in parallel using pirmers: 5′ GTAACCCGTTGAACCCCATT 3′ (rat Rn18S-specific forward primer) and 5′ CCATCCAATCGGTAGTAGCG 3′ (rat Rn18S-specific reverse primer). PCR amplifications were performed using a CFX96 Touch Real-Time PCR detection system (Bio-Rad Laboratories). For data analysis and analysis CFX Manager Software version 3.1 (Bio-Rad Laboratories) was used.

Western Blotting

Cells were washed 3 times with ice-cold PBS and lysed on ice in RIPA buffer (50 mM Tris–HCl [pH=8.0], 150 mM NaCl, 1% Triton X-100, 0.5% sodium deoxycholate, 0.1% sodium dodecyl sulfate supplemented with protease inhibitors [cOmplete, Mini Protease Inhibitor Cocktail Tablet; Roche Applied Science, Penzberg, Germany]). After centrifugation of the cell lysate for 15 min at 21,130 × *g* and 4ºC, the supernatant was collected, passed 3 times through a 29 Gauge needle (BD Biosciences), aliquoted and stored at -80ºC until assay. Protein concentration was determined using the BCA protein assay kit (Thermo Fisher Scientific). Proteins were size-fractionated in Novex Bolt 8% Bis-Tris Plus gels (Life Technologies) and transferred to Amersham Hybond-N$^+$ polyvinylidene difluoride membranes (GE Healthcare, Diegem, Belgium) by wet electroblotting using a Bolt Mini Blot Module (Life Technologies). After blocking for 1 h in 2% ECL Prime blocking reagent (GE healthcare) dissolved in Tris-based saline/0.1% Tween-20 (TBST), membranes were incubated for 1 h with primary antibodies directed against Cx43 (Gja1 gene product; 1:100,000; rabbit IgG, polyclonal; Sigma-Aldrich) or lamin A/C (Lmna gene product; 1:5,000; rabbit IgG, polyclonal; Santa Cruz Biotechnology) as an internal control. All antibodies were diluted in TBST/2% ECL Prime blocking reagent. After 3 washes with TBST, blots were incubated with corresponding horseradish peroxidase-conjugated secondary antibodies (1:25,000; donkey-anti-rabbit IgG-HRP, Santa Cruz Biotechnology) for 1 h at RT. After another 3 wash steps with TBST, membranes were immersed in SuperSignal West Femto Maximum Sensitivity substrate (Thermo Scientific) and chemiluminescence was measured with the ChemiDoc XRS imaging system (Bio-Rad Laboratories). Dedicated software was used for imaging and quantification.

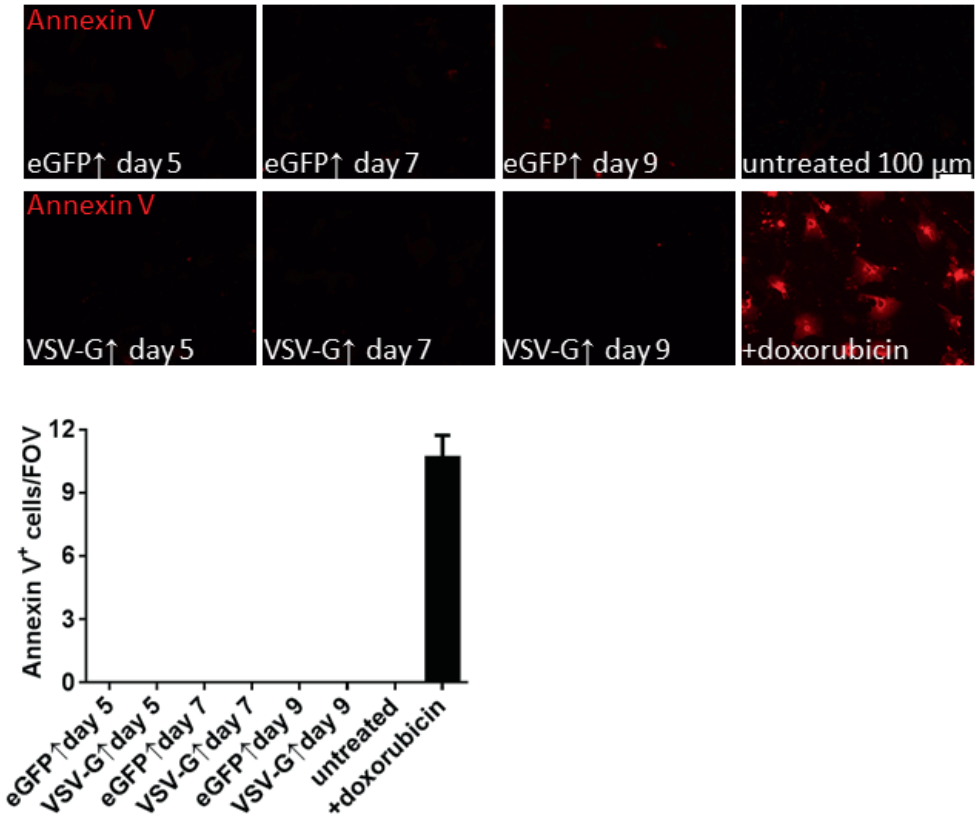

Supplementary Figure S4. Assessment of the viability of eGFP↑-co-cultures (eGFP↑) and fused VSV-G/eGFP↑-co-cultures (VSV-G↑) by live cell staining for externalized phosphatidylserine as early marker of apoptosis. On day 5, 7 and 9 of culture, *i.e.* at 2, 4 and 6 days after the induction of intercellular fusion, the cells were incubated with Alexa Fluor 568-conjugated annexin V and the number of fluorescently labelled cells per field of view (FOV) was determined. NRVM cultures that were incubated for 24 h with 1 mM doxorubicin (Sigma-Aldrich) or its solvent (untreated) served a positive and negative controls, respectively. The quantitative data are based on 3 independent experiments and 20 images.

Apoptosis assay

Apoptosis in our cell cultures was assessed by labeling with Alexa Fluor 568-conjugated annexin V (Life Technologies). Cells were cultured on glass coverslips in 24-well cell culture plates as described previously, and assays were performed on day 5, 7 and 9 of culture, *i.e.* at 2, 4 and 6 days after the induction of intercellular fusion. Cells were washed once with ice-cold PBS and immediately afterwards incubated for 15 min at RT and in the dark with Alexa Fluor 568-conjugated annexin V (diluted 1:20 in homemade binding buffer) as recommended by the manufacturer. The binding buffer consisted of 10 mM HEPES, 140 mM NaCl, and 2.5 mM $CaCl_2$ and was set at pH 7.4 with NaOH solution. Next, the cell cultures were washed once with ice-cold binding buffer, which was replaced by PBS for live cell imaging using a Leica

DMI6000 B inverted microscope (Leica Microsystems) equipped with a color camera and dedicated software. To generate positive control samples, NRVM cultures were treated with 1 mM doxorubicin (Sigma-Aldrich) during 24 h immediately prior to assay.

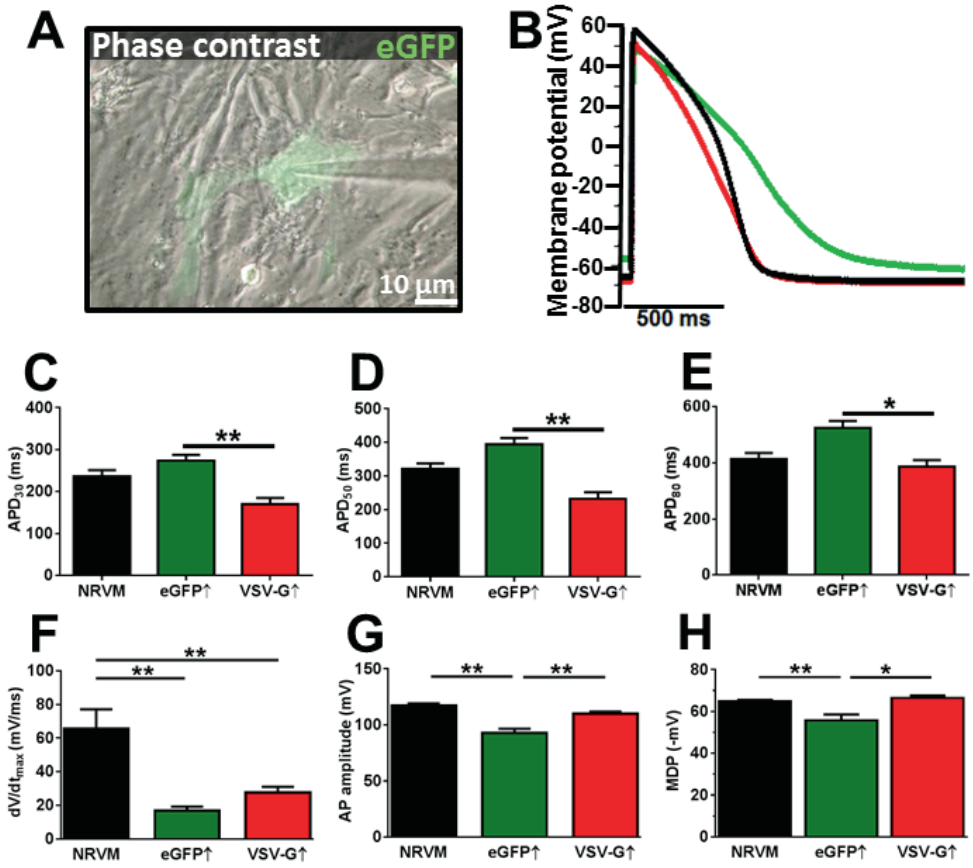

Supplementary Figure S5. Effect of heterocellular fusion on AP characteristics assessed in confluent monolayer cultures by the perforated-patch WC patch-clamp technique. (*A*) Typical example of a VSV-G/eGFP↑-co-culture after induction of fusion showing an eGFP$^+$ (eGFP; green) heterokaryon with the patch-pipette attached to its surface. (*B*) Overlay of typical AP recordings of an NRVM in a NRVM culture (black), of a NRVM in a 4:1 configuration with hVSCs in an eGFP↑-co-culture (green) and of a heterokaryon surrounded by NRVMs in a VSV-G/eGFP↑-co-cultures (red). Quantification of APD at (*C*) 30% repolarization (APD_{30}), (*D*) 50% repolarization (APD_{50}) and (*E*) 80% repolarization (APD_{80}), (*F*) maximum upstroke velocity (dV/dt_{max}), (*G*) AP amplitude and (*H*) maximum diastolic potential (MDP), as measured by perforated patch recordings in NRVM cultures (black; N=8), eGFP↑-co-cultures (green; N=7) and VSV-G/eGFP↑-co-cultures (red; N=10).

Optical voltage mapping

Assessment of the effects of heterocellular fusion on cardiac electrical impulse propagation in monolayers was done by optical mapping 48 h after fusion induction. Cells were loaded with voltage-sensitive dye by incubation for 15 min at 37ºC in a humidified incubator (95% air/5% CO_2) with serum-free and phenol red-less DMEM/Ham's F12 medium (1:1, v/v; DMEM/F12; Life Technologies) containing 8 µM di-4-ANEPPS (Life Technologies). After replacement of the staining solution with fresh unsupplemented DMEM/F12, mapping experiments were performed with a MiCAM ULTIMA-L imaging system (SciMedia, Costa Mesa, CA). Cells were stimulated electrically with an epoxy-coated bipolar platinum electrode with square 10 ms, 8 V suprathreshold electrical stimuli using a STG 2004 stimulus generator and MC Stimulus II software (both from Multichannel Systems, Reutlingen, Germany). Optical signals were recorded at a 6-ms frame rate and analyzed using BrainVision Analyzer 13.04.20 software (Brainvision, Tokyo, Japan), after spatial and temporal filtering. Upon 1-Hz pacing, cell cultures were assessed for conduction velocity (CV), action potential (AP) duration (APD) at 50% and 80% of full repolarization (APD_{50} and APD_{80}, respectively), APD dispersion of repolarization and early afterdepolarization (EAD) incidence. APD dispersion was calculated as the maximal temporal difference in APD_{80} within one culture. EADs were defined as one or more abnormal depolarizations during phase 2 or 3 of the AP during 1-Hz electrical pacing. EADs were quantified by calculating the percentage of cultures that showed one or more EADs upon 1-Hz pacing during optical mapping assay. To study the effects of outward K_v current blockade, cultures were incubated for 10 min in NRVM culture medium containing 40 mM tetraethylammonium (TEA; Sigma-Aldrich) or 1 mM 4-aminopyridine (4-AP; Sigma-Aldrich) and subjected to electrophysiological measurements immediately afterwards.

Patch-clamp recordings

Patch-clamp measurements were conducted on day 5 of culture at 20-23°C with a conventional system consisting of a MultiClamp 700B amplifier and a Digidata 1440A A/D converter, controlled by Clampex 10 software (Axon CNS, Molecular Devices, Sunnyvale, CA).

To manufacture patch pipettes, borosilicate glass capillaries (1.5 mm outer diameter and 1.17 mm inner diameter; Harvard Apparatus, Kent, United Kingdom) were pulled by a model P-30 vertical micropipette puller (Sutter Instrument Company, Novato, CA). When filled with pipette solution, pipettes showed a typical resistance of 2-3 MΩ. Whole-cell (WC) current-clamp recordings were performed on single NRVMs, single hVSCs and isolated heterokaryons in cultures that had been previously subjected to a brief low pH treatment to induce VSV-G-dependent intercellular fusion. The pipette solution consisted of (in mM): 80 potassium DL-aspartate, 40 KCl, 8 NaCl, 5.5 glucose, 5 HEPES, 5 EGTA, 1 $MgCl_2$, 4 Mg-ATP, and 0.1 Na_3-

GTP (adjusted to pH 7.20 with KOH). Unless mentioned otherwise, cells were bathed in an extracellular solution composed of (in mM): 126 NaCl, 11 glucose, 10 HEPES, 5.4 KCl, 1 $MgCl_2$, and 1.8 $CaCl_2$ (adjusted to pH 7.40 with NaOH).

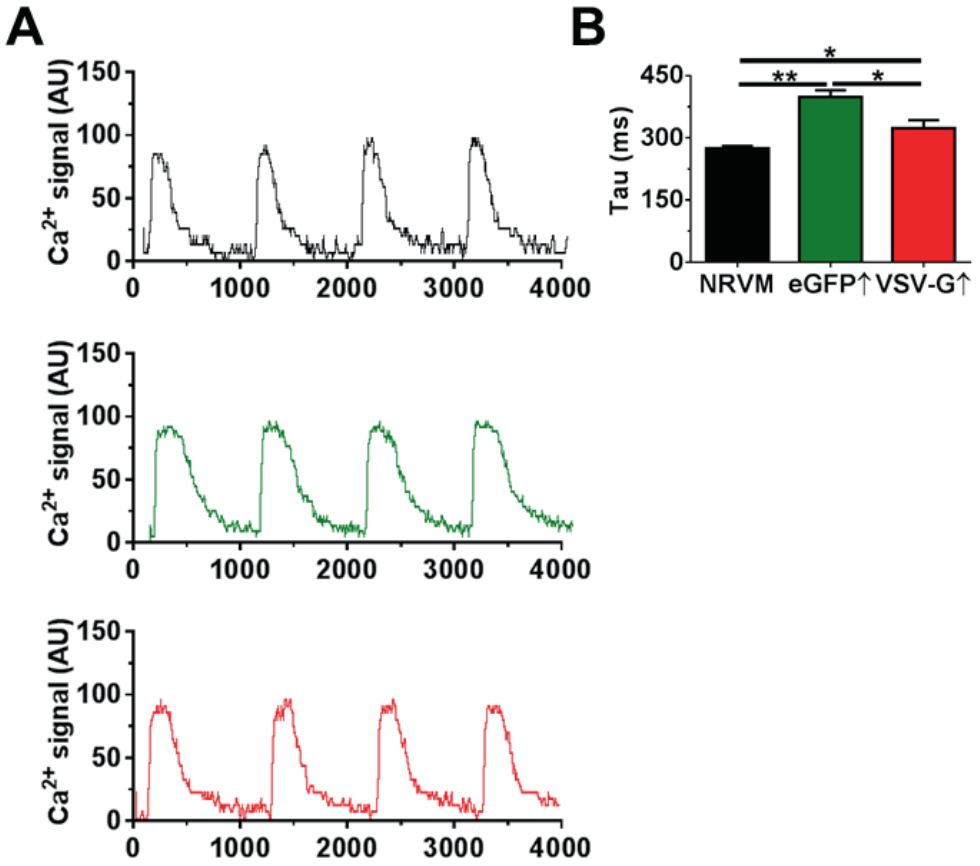

Supplementary Figure S6. Measurement of Ca^{2+} transient dynamics in confluent monolayer cultures by optical mapping using the Ca^{2+} indicator Rhod-2-AM. (*A*) Typical Ca^{2+} signal traces for a NRVM culture (upper panel; black), an eGFP↑-co-culture (middle panel: green) and a VSV-G/eGFP↑-co-culture (lower panel: red). (*B*) Comparison of the times at which the cytosolic Ca^{2+} concentration had decreased to 63% of its peak value ($\tau_{63\%}$). N=10 for the NRVM cultures, N=9 for the eGFP↑-co-cultures and N=9 for the VSV-G/eGFP↑-co-cultures.

To study the effects of Kv current inhibition, cells were perfused with extracellular solutions consisting of (in mM): 11 glucose, 10 HEPES, 5.4 KCl, 1 $MgCl_2$, 1.8 $CaCl_2$ and either 40 TEA plus 86 NaCl or 1 4-AP plus 126 NaCl. The pH of these solutions was adjusted to 7.40 with NaOH. Whole-cell capacitance (C_m) was calculated from capacitive transient currents evoked during 5 mV steps from a holding potential of -50 mV using the membrane test feature of pClamp 10

software. Subsequently, C_m and the series resistance (>75%) were compensated electronically. C_m was used as a measure of cell size for current normalization.

Monolayer recordings were performed in confluent cultures on spontaneously active cells using a perforated patch-clamp method.[9] Recordings encompassed NRVMs in NRVM cultures, NRVMs adjacent to eGFP-expressing hVSCs in eGFP↑-co-cultures and heterokaryons in VSV-G/eGFP↑-co-cultures. Each of these cell cultures had been exposed for 3.5 min to culture medium of pH 6.0, 48 hours before patch clamping. An ATP- and GTP-free pipette solution was used to tip-fill patch pipettes, and an ATP- and GTP-free pipette solution containing nystatin (120-200 µg/mL; Sigma-Aldrich) was used to back-fill the pipettes. Recordings were started after the series resistance had reached steady state and the AP amplitude was stable (*i.e.* after 20-30 min). The integrity of the perforated patch was checked during and after recording for every experiments to ensure reliability of recordings. Data were sampled at intervals of 100 µs and low-pass filtered at 2-4 kHz with a four-pole Bessel filter. The calculated liquid junction potential (~11 mV) between pipette and bath solution was only compensated for in the case of resting membrane potential measurements of single cells. Data analysis was carried out with Clampfit 10 software (Axon CNS, Molecular Devices).

Statistical analysis

Statistical analyses were performed using GraphPad Prism software version 6 (Graphpad Software, La Jolla, CA). Unpaired Student's t test, Fisher's exact test and the one-way ANOVA test were used for comparing different experimental groups. Data were expressed as mean±standard error of mean (SEM) for a specified number (N) of observations. Results were considered statistically significant at P values <0.05. Statistical significance was expressed as follows: *: P<0.05, **: P<0.01, ***: P<0.001, NS: not significant.

Results

Ionic membrane currents in heterokaryons

In order to explore the anti-arrhythmic mechanisms of heterocellular fusion in more detail, patch-clamp experiments were conducted to compare whole-cell (WC) membrane current profiles of single NRVMs, single hVSCs and isolated heterokaryons. NRVMs showed voltage-step evoked WC-currents, typical for these excitable cells (*Figure S7A*).[10,11] Inward rectifier currents (I_{Kir}) were observed upon hyperpolarizing voltage steps below -80 mV (*Figure S7A, D, E*). Fast transient inward currents were recorded upon depolarizing voltage steps from a holding voltage of -80 mV to voltages >-50 mV (Figure S7A, D). These currents were mainly voltage-

activated sodium currents (I_{Nav}), based on their fast time course, complete inhibition by 30 nM tetrodotoxin (TTX) (N=20, data not shown) and inactivation at -40 mV. The latter property was used to unmask the presence of voltage-activated L-type Ca^{2+} currents in the records (I_{CaL}; *Figure S7A inset and F*). The complete inhibition of these currents by 10 μM nitrendipine (N=8, data not shown) confirmed their identity. T-type Ca^{2+} currents were not investigated, because these currents are of minor importance in NRVMs.[12] Relatively small depolarization-activated outward currents (I_{ov}) could be evoked upon steps to voltages > 0mV. These currents are best recognized at voltages where the other currents are close to zero (main manuscript *Figure 6* and Figure *S7A, D and E*). The mean peak current-voltage (I-V) relationship of the total NRVM WC-current densities shows the typical I-V profile of these cells (*Figure S7D*).

In contrast to NRVMs, WC-current records and I-V profiles of hVSCs showed absence of I_{Kir}, I_{Nav} and I_{CaL}, but presence of I_{ov}, consistent with inexcitable cell properties (*Figure S7B, D*).

The WC current-records of heterokaryons were not simple proportional additions of those of NRVMs and hVSCs. Upon stimulation with a defined current pulse, about half of the heterokaryons responded by eliciting an AP (main manuscript, *Figure 3C*). In current records of responsive heterokaryons, I_{Kir}, I_{Nav}, I_{CaL} and I_{ov} could be easily recognized (*Figure S7C with inset, D, F*). I_{Kir} was strongly diluted and I_{Nav} showed smaller current densities compared to NRVMs. This current could, however, not be evaluated quantitatively, because a reliable measurement of this current was not feasible in cells with such large C_m, as apparent from its slow time course. Peak I_{CaL} was much less diluted than I_{Kir} (*Figure S7F*). The peak I_{ov} density of the heterokaryons was similar to that of hVSCs at all positive potentials and to that of NRVMs around 50 mV (Figure S7G). The average I_{ov} density of heterokaryons was clearly increased at all positive potentials (*Figure S7H*) and showed an overall slower inactivation time course in comparison with NRVMs and hVSCs (main manuscript, *Figure 6B-C*). Pooled results show I-V curve profiles between that of responsive heterokaryons and hVSCs (*Figure S7D, F*). We concluded that I_{ov} was mainly Kv-current, as it was largely inhibited by 40 mM external TEA (main manuscript, *Figure 6D-E*), while inhibition by 1 mM 4-AP was ~30% (N=6, data not shown). Taken together, these data show that heterokaryons share cardiomyocytic and fibroblastic currents to a variable degree, with cardiomyocytic I_{Kir} density being most diluted by the heterocellular fusion, with I_{CaL} being upregulated for partial compensation of the dilution and with the average heterocellular I_{Kv} density being larger than I_{Kv} of hVSCs and of NRVMs. Thus, NRVMs contribute elements of excitability to the heterokaryons, while hVSCs contribute increased repolarization force to these fused cells.

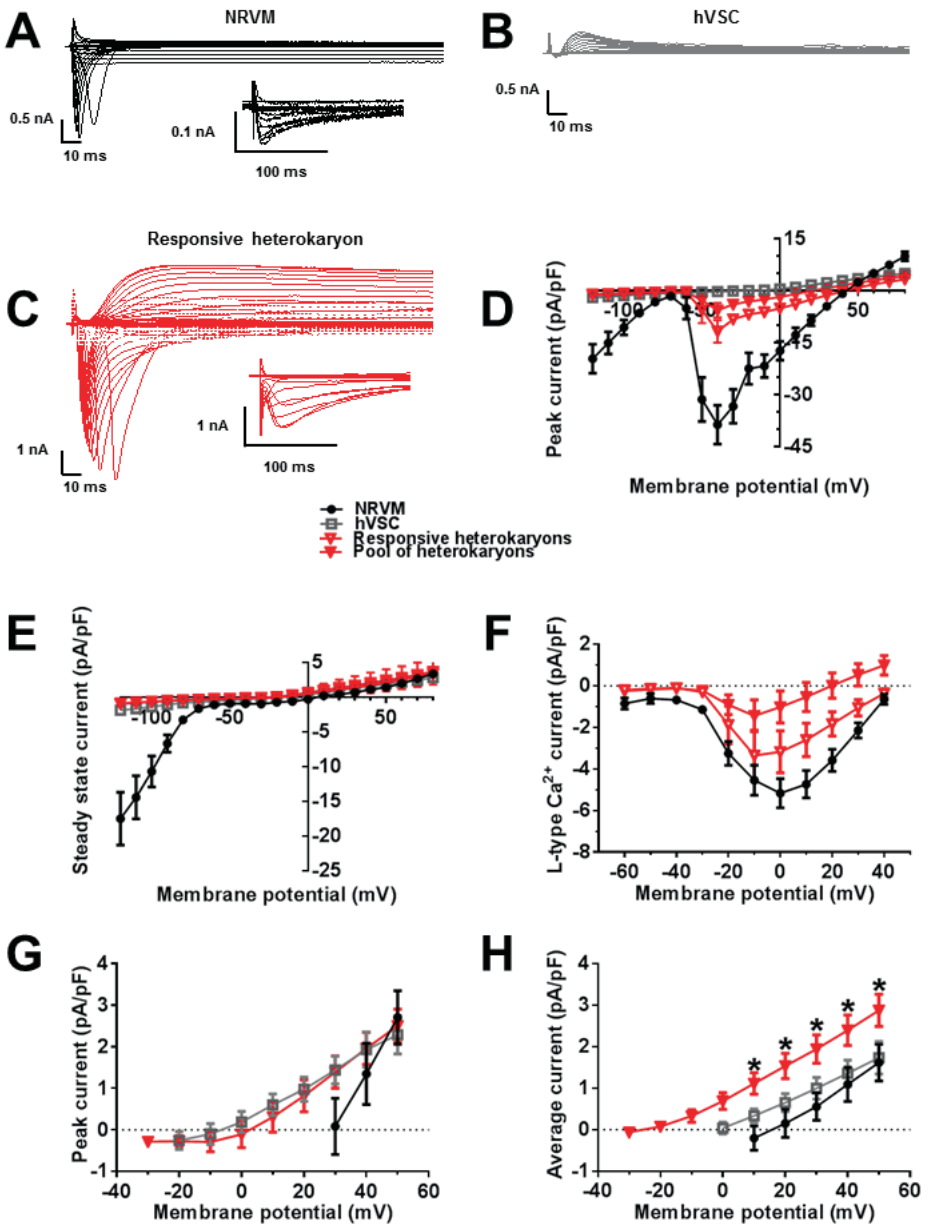

Supplementary Figure S7. Membrane current profiles of single NRVMs, single hVSCs and solitary heterokaryons. Families of representative whole-cell current recordings of an (*A*) NRVM, (*B*) hVSC and (*C*) responsive heterokaryon. To obtain the recordings in *A-C*, 400-ms voltage pulses between -120 and +80 mV were applied in 10-mV increments every 5 s from the holding potential (Vh) = -80 mV. Calcium-current ($I_{Ca,L}$) traces in inset *A* and inset *C* were recorded at Vh = -40 mV to fully inactivate voltage dependent Na^+ current (I_{Nav}), and the test pulses were from -60 mV to 40 mV with 10 mV increases, separated by 5-s rest intervals. Voltage-current (I-V) relationship of the (*D*) total peak and (*E*) steady state current

density were expressed as the mean±SEM and measured from NRVMs (filled black circle; N=9), hVSCs (filled grey square; N=9), responsive heterokayons (open red triangle; N=7) and pool of heterokaryons (filled red triangle; N=15). *D* was obtained from the current amplitudes at the beginning of each voltage step, and *E* was obtained from steady state currents at the end of 400-ms test pulses. (*F*) I-V relationships of $I_{Ca,L}$ are plotted at each test potential as mean±SEM obtained from NRVMs (filled black circle; N=7), responsive heterokayons (open red triangle; N=5) and the pool of heterokaryons (filled red triangle; N=11). I-V relationships of the (*G*) peak outward current were taken at 50-ms after depolarization and the (*H*) average outward current was calculated from 50-ms till 400-ms prior to repolarization from single NRVMs (filled black circle; N=9), single hVSCs (filled grey square; N=9) and isolated pooled responsive and non-responsive heterokaryons (filled red triangle; N=8 for each group).

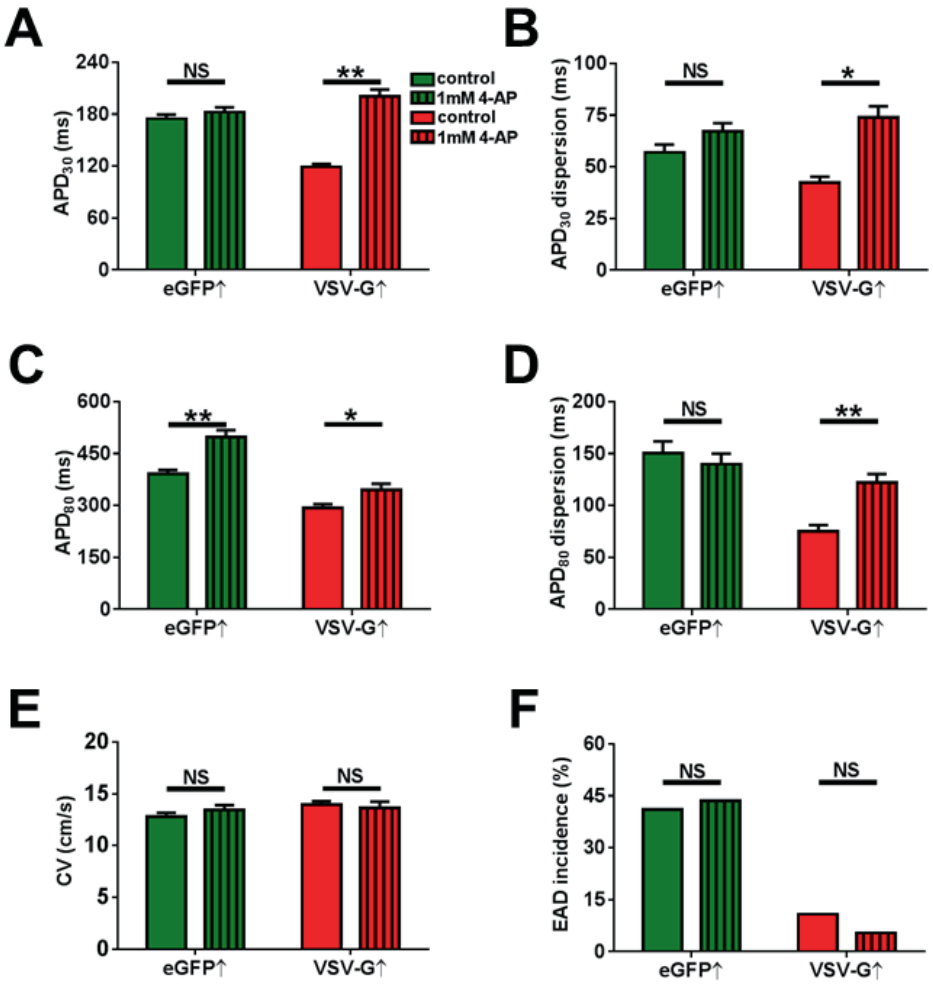

Supplementary Figure S8. Evaluation of the effects of 4-AP on the electrophysiological properties of eGFP↑-co-cultures and fused VSV-G/eGFP↑-co-cultures by optical voltage mapping. Effect of 4-AP or vehicle (control) in unfused (eGFP↑; green, both N=8) and fused (VSV-G↑; red, both N=9) fibrotic NRVM cultures on (*A*) APD_{30}, (*B*) APD_{30} dispersion, (*C*) APD_{80}, (*D*) APD_{80} dispersion, (*E*) CV and (*F*) EAD incidence.

References

1. van Tuyn J, Pijnappels DA, de Vries AA, de Vries I, van der Velde-van Dijke I, Knaan-Shanzer S, van der Laarse A, Schalij MJ, Atsma DE. Fibroblasts from human postmyocardial infarction scars acquire properties of cardiomyocytes after transduction with a recombinant myocardin gene. *FASEB J.* 2007;21:3369-3379.
2. Pijnappels DA, van Tuyn J, de Vries AA, Grauss RW, van der Laarse A, Ypey DL, Atsma DE, Schalij MJ. Resynchronization of separated rat cardiomyocyte fields with genetically modified human ventricular scar fibroblasts. *Circulation.* 2007;116:2018-2028.
3. Green MR, Schaefer JA. Molecular Cloning: A Laboratory Manual. In: Cold Spring Harbor Laboratory Press, 2012.
4. Vellinga J, Uil TG, de Vries J, Rabelink MJ, Lindholm L, Hoeben RC. A system for efficient generation of adenovirus protein IX-producing helper cell lines. *J Gene Med.* 2006;8:147-154.
5. Bingen BO, Neshati Z, Askar SF, Kazbanov IV, Ypey DL, Panfilov AV, Schalij MJ, de Vries AA, Pijnappels DA. Atrium-specific Kir3.x determines inducibility, dynamics, and termination of fibrillation by regulating restitution-driven alternans. *Circulation.* 2013;128:2732-2744.
6. Askar SF, Ramkisoensing AA, Atsma DE, Schalij MJ, de Vries AA, Pijnappels DA. Engraftment patterns of human adult mesenchymal stem cells expose electrotonic and paracrine proarrhythmic mechanisms in myocardial cell cultures. *Circ Arrhythm Electrophysiol.* 2013;6:380-391.
7. Askar SF, Ramkisoensing AA, Schalij MJ, Bingen BO, Swildens J, van der Laarse A, Atsma DE, de Vries AA, Ypey DL, Pijnappels DA. Antiproliferative treatment of myofibroblasts prevents arrhythmias in vitro by limiting myofibroblast-induced depolarization. *Cardiovasc Res.* 2011;90:295-304.
8. Engels MC, Rajarajan K, Feistritzer R, Sharma A, Nielsen UB, Schalij MJ, de Vries AA, Pijnappels DA, Wu SM. Insulin-like growth factor promotes cardiac lineage induction in vitro by selective expansion of early mesoderm. *Stem Cells.* 2014;32:1493-1502.
9. Akaike N, Harata N. Nystatin perforated patch recording and its applications to analyses of intracellular mechanisms. *Jpn J Physiol.* 1994;44:433-473.
10. Fermini B, Schanne OF. Determinants of action potential duration in neonatal rat ventricle cells. *Cardiovasc Res.* 1991;25:235-243.
11. Deschenes I, Armoundas AA, Jones SP, Tomaselli GF. Post-transcriptional gene silencing of KChIP2 and Navbeta1 in neonatal rat cardiac myocytes reveals a functional association between Na and Ito currents. *J Mol Cell Cardiol.* 2008;45:336-346.
12. Avila G, Medina IM, Jimenez E, Elizondo G, Aguilar CI. Transforming growth factor-beta1 decreases cardiac muscle L-type Ca2+ current and charge movement by acting on the Cav1.2 mRNA. *Am J Physiol Heart Circ Physiol.* 2007;292:H622-H631.